AD-A042 435 AIR FORCE FLIGHT DYNAMICS LAB WRIGHT-PATTERSON AFB OHIO F/G 13/5
LOAD SPECTRUM EFFECTS ON BONDED COMPOSITE JOINTS.(U)
APR 77 R T ACHARD, M D RICHARDSON
UNCLASSIFIED AFFDL-TR-77-29 NL

1 OF 2
AD A042435

AFFDL-TR-77-29

12

LOAD SPECTRUM EFFECTS ON BONDED COMPOSITE JOINTS

STRUCTURAL CONCEPTS BRANCH
STRUCTURAL MECHANICS DIVISION

APRIL 1977

TECHNICAL REPORT AFFDL-TR-77-29
FINAL REPORT FOR PERIOD JANUARY 1972 to DECEMBER 1976

AIR FORCE FLIGHT DYNAMICS LABORATORY
AIR FORCE WRIGHT AERONAUTICAL LABORATORIES
AIR FORCE SYSTEMS COMMAND
WRIGHT-PATTERSON AIR FORCE BASE, OHIO 45433

NOTICE

When Government drawings, specifications, or other data are used for any purpose other than in connection with a definitely related Government procurement operation, the United States Government thereby incurs no responsibility nor any obligation whatsoever; and the fact that the government may have formulated, furnished, or in any way supplied the said drawings, specifications, or other data, is not to be regarded by implication or otherwise as in any manner licensing the holder or any other person or corporation, or conveying any rights or permission to manufacture, use, or sell any patented invention that may in any way be related thereto.

This report has been reviewed by the Information Office (OI) and is releasable to the National Technical Information Service (NTIS). At NTIS it will be available to the general public, including foreign nations.

This technical report has been reviewed and is approved for publication.

Robert T. Achard

ROBERT T. ACHARD
Project Engineer

FOR THE COMMANDER

Larry G. Kelly

LARRY G. KELLY
Acting Chief
Advanced Structures Development Branch
Structural Mechanics Division

Copies of this report should not be returned unless return is required by security considerations, contractual obligations, or notice on a specific document.

AIR FORCE - 28 JUN 77 - 125

SECURITY CLASSIFICATION OF THIS PAGE (When Data Entered)

REPORT DOCUMENTATION PAGE

READ INSTRUCTIONS BEFORE COMPLETING FORM

1. REPORT NUMBER: AFFDL-TR-77-29	2. GOVT ACCESSION NO.
3. RECIPIENT'S CATALOG NUMBER	
4. TITLE (and Subtitle): Load Spectrum Effects on Bonded Composite Joints	5. TYPE OF REPORT & PERIOD COVERED: Final Report for Period Jan 1972 to Dec 1976
	6. PERFORMING ORG. REPORT NUMBER
7. AUTHOR(s): R. T. Achard and M. D. Richardson	8. CONTRACT OR GRANT NUMBER(s)
9. PERFORMING ORGANIZATION NAME AND ADDRESS: Air Force Flight Dynamics Laboratory, Wright-Patterson Air Force Base, Ohio 45433	10. PROGRAM ELEMENT, PROJECT, TASK AREA & WORK UNIT NUMBERS
11. CONTROLLING OFFICE NAME AND ADDRESS: Air Force Flight Dynamics Laboratory, Wright-Patterson Air Force Base, Ohio 45433	12. REPORT DATE: April 1977 13. NUMBER OF PAGES: 95
14. MONITORING AGENCY NAME & ADDRESS (if different from Controlling Office)	15. SECURITY CLASS. (of this report): Unclassified
	15a. DECLASSIFICATION/DOWNGRADING SCHEDULE

16. DISTRIBUTION STATEMENT (of this Report)

Approved for public release; distribution unlimited

17. DISTRIBUTION STATEMENT (of the abstract entered in Block 20, if different from Report)

18. SUPPLEMENTARY NOTES

19. KEY WORDS (Continue on reverse side if necessary and identify by block number)

Bonded Joints
Advanced Composite
Flight-by Flight Loads
Load Spectrum Effects
Fatigue
Aircraft Structures

20. ABSTRACT (Continue on reverse side if necessary and identify by block number)

This report presents the results of an experimental study of the fatigue and residual strength behavior of double lap boron/epoxy-to-titanium bonded joints. The program investigated various effects of load spectrum truncation, frequency, and intensity, and surface ply orientation on specimen endurance at a room temperature, dry environment.

Results indicate the sensitivity of fatigue life to the orientation of the plies at the bond surface. Low amplitude loads, approximately lg about the

(continued on the back)

DD FORM 1 JAN 73 1473 EDITION OF 1 NOV 65 IS OBSOLETE

SECURITY CLASSIFICATION OF THIS PAGE (When Data Entered)

mean, were significant and should not be arbitrarily truncated. Proof loading to 130% of limit load significantly reduced fatigue life even where spectrum loads were of this same magnitude. Fully random load sequencing was found to reduce the endurance or flight-by-flight missions to failure over a contrived but reasonably random spectrum that contained blocked loading (constant amplitude) of low intensity loads. The location of the scrim material on each boron/epoxy ply played a significant role in the strength and failure mode of the joints. The frequency of applying random loads was not significant, comparing 1/2 Hz and 8 Hz endurance data.

FOREWORD

This program was initiated to develop screening data on the effects of load frequency, spectrum, truncation and lamination orientation on advanced composite bonded joints. Mr. R. T. Achard was the project engineer, data analyst, and writer of the manuscript. Mr. M. D. Richardson was the test engineer on the program. Other contributors in the Structural Mechanics Division of the Air Force Flight Dynamics Laboratory included Messrs J. G. Anderson and N. K. Mondal in the area of load spectra generation, Mr. H. F. Ostroski on equipment procurement and repair, Mr. R. Ditmer, who conducted many of the tests, and Mr. W. Leisler, who operated the Scanning Electron Microscope. Specimens were fabricated and quality controlled by Mr. G. Jenkins of Monsanto Research Corporation. Manuscript typing and layout were by Mrs. E. Calloway and Miss C. S. Hardin.

The program was conducted between January 1972 and December 1976. The final report was released in March 1977.

TABLE OF CONTENTS

TABLE OF CONTENTS (CONT'D)

LIST OF ILLUSTRATIONS

LIST OF ILLUSTRATIONS (CONT'D)

LIST OF TABLES

SECTION I

INTRODUCTION

The joining of composite structural elements to metals or other composites is one of the most significant aspects of advanced composite airframe design. In theory, adhesive bonding is a most efficient approach. Although adhesive bonding eliminates many of the problems associated with stress concentrations at point attachments (such as found in conventional mechanical joints), this type of joint is subject to stress concentrations near the bond edges. Furthermore, a variety of failure modes are possible in the bond and laminated adherend areas of a bonded composite joint. The problem of adhesive joint design is compounded for fatigue-critical applications, especially for primary-load-carrying structures where heavy, overdesigned composite concepts may be employed; or where the application of composites may be rejected altogether for lack of confidence in bonded joint behavior.

Methods to predict composite joint reliability or life under flight loading using constant-amplitude-coupon-fatigue data have been generally unsatisfactory. On the other hand, multiple full-scale structural testing, incorporating real-time load simulation plus realistic environmental effects, tends to be impractical due to both excessive costs and test times. These factors are particularly troublesome in the design of advanced composite structures where a large backlog of flight-hardware experience does not exist, and manufacturing methods and materials are undergoing rapid developmental changes. One approach to providing a rational engineering design for fatigue-critical composite joints is to develop a residual strength model. This approach is discussed in

Reference 1 and 2. Efficient implementation of this type of concept involves (a) the development of adequate design and reliability data from small scale structures under time-compressed loading, and subsequently (b) the adjustment of this empirical data for the effects of complexity, scale, environment, real-time loading, etc. If successful, these procedures would then provide an analytical model for joint sizing, design, and reliability prediction. Such an approach becomes attractive if relationships can be developed between the statistical parameters for initial static strength, residual static strength after various fatigue histories, and time-to-failure distributions; and if the sensitivity of the statistical parameters to specimen scale and test parameters can be readily determined or estimated. Experimental efforts are needed to verify this design and reliability-assessment methodology, and to generate the qualitative and quantitative data necessary to implement the concepts into design criteria and the various stages of structural design and compliance demonstration. Furthermore, the sensitivity of this methodology to the degree of sophistication in such factors as environment and loading simulation, must be determined and incorporated into practical methodology.

This experimental program was initiated in 1971 to explore the effects of load frequency, type of load sequencing, load truncation, and load magnitude on the failure characteristics of elementary adhesively bonded composite-to-metal joints. Random, flight-by-flight tests simulating the loads on a lower-wing-cover splice of a fighter-bomber were conducted, and the data were obtained on a time-to-failure,

residual strength, joint overlap extension under load, and failure modes. Two joint designs were evaluated. These differed only by the ply arrangement of the composite adherend. The joints, classified as Schedule 40 and Schedule 50, respectively, are described in the following section.

Progress on the program was restricted by the in-house availability of test apparatus, with testing being conducted over approximately three years. During this period significant work on joint design (References 3 & 4) and fatigue (Reference 4) has been conducted elsewhere and the findings of this program were integrated into the planning of various AFFDL programs (References 5 & 6). Data from the contemporary efforts are compared in this report to the findings of this study.

SECTION II

SPECIMEN DESIGN

The specimen design for this program is detailed in Figure 1. Test coupons were designed to achieve a static ultimate load of approximately 6,000 lb per inch of width, based upon an average shear strength for the adhesive of 6,000 psi over a 1/2 inch lap length on the double lap specimens. Unlike normal airframe practice, where the joint is designed to be stronger than the joined structure, failure for these specimens was to occur in the joint. Also, the safety margins normally applied to bonded joints to account for strength degradation with age and environment were omitted from the design of these specimens to assure joint failure within a reasonable test time.

Composite material on hand at the beginning of the program constrained the composite thickness to approximately .08 inch. Two balanced and symmetrical 16 ply boron-epoxy panels, 50% 0°, 50% $\pm$ 45°, fabricated by General Dynamics/Fort Worth from Narmco 5505 were used. As shown in Figure 1, one panel had 0° exterior plies, and therefore a 0° ply on each faying surface of the specimen. These are hereafter referred to as Schedule 40 specimens. The other panel had $\pm$ 45° surface plies. Specimens fabricated from this panel are named Schedule 50. For all specimens, 0° is in the direction of the applied load. The two boron-epoxy panels used in the program were analyzed by H_2SO_4/H_2O_2 digestion to have the following constituents:

SCHEDULE	40	50
Specific Gravity	1.98	1.99
Boron Wgt. %	64.8	65.9
Glass Wgt. %	5.4	5.1
Resin Wgt. %	29.8	29.0
Boron Vol. %	48.7	49.6
Glass Vol. %	4.3	4.1
Resin Vol. %	46.8	45.7
Void Vol. %	0.2	0.6

The joint design was not exactly balanced respecting equal stiffness (modulus times thickness) between adherends. Based upon a stiffness ratio ($2E_{Ti}\ t_{Ti} \div E_{B/E}\ t_{B/E}$) of 1.32 for the titanium (Ti) to composite (B/E), and the design curves of Hart-Smith (Reference 3) one would expect that 96% of the maximum bond line strength would result.

The nominal tensile strength of the boron composite was estimated at 9152 lb per inch of width (110 ksi), and the titanium yield was 16,100 lb per inch.

The specimen was designed to contain two double lap joints; one with a 1/2 inch lap and the other with a 3/4 inch lap. The shorter joint was to fail during cyclic loading, and the larger lap was included to provide an unfailed joint after the fatigue failure of the 1/2 inch lap. This 3/4 inch joint was subsequently to be tested for a residual strength comparison with the initial strength of the joint. (It was subsequently found, however, that the fatigue failure in the smaller joint was not assured.) Although the strength of the boron laminate was close to the estimated initial strength of the virgin 3/4 inch lap, it was expected that a degradation in strength during fatigue would force most residual strength failures to occur in the joint and not the laminate outside the joint.

The specimens included a 1 inch aluminum spacer between the two joints to allow gripping for the residual strength testing of the 3/4 inch joints.

SECTION III

SPECIMEN FABRICATION

The double lap specimens of this program were fabricated in February 1972 by conventional autoclave bonding in long slabs or gangs by the Monsanto Research Corporation of Dayton, Ohio. All components shown in Figure 1 were bonded in one operation. After trim operations of the first cut edge, which removed 1/2 inch, specimens of 0.5 and 1.0 inch width were sliced with a diamond cut-off wheel. A typical specimen is shown in Figure 2. The locations of the 0.5 inch wide specimens were generally at the two ends of the trimmed slab and in the center of the gang. These locations were in accordance with plans to investigate location effects. Five steel fixtures were fabricated to bond all precured components (including tabs) in one operation. Curing in the program was accomplished in five autoclave runs: heat up rate - 2 F/min, cure pressure - 50 psi; temperature - 1 hour at 350 F. The bonding tool elements and component stacking for the specimens were in accordance with Figure 3.

The procedures for cleaning and treating the titanium and composite surfaces included the following for both the titanium and composite components: acetone wipe, 120 grit orbital sanding, perchloroethylene vapor degrease (15 minutes). In addition, the titanium received a sodium metasilicate/sodium fluoride solution etch (5 minutes), with associated rinses. Parts were bonded immediately after oven drying at 175 F for 15 minutes.

Specimens were sliced on a horizontal mill without any finish operations. A diamond cutting wheel (Norton/80 grit/6 inches dia/copper matrix) was run at 1800 rpm with a feed of approximately one inch per minute. Water flood

coolant was used. Observed tolerances were ±0.7% on width and generally ±0.3% on bond area. Titanium sheet purchased for the program was annealed 6Al-4V alloy with the sheet thickness averaging 0.058 inches. Both precured boron epoxy sheets averaged .086 inches.

Numbering of specimens was related to the particular autoclave run, fixture, and location on the fixture, i.e., consecutive numbers in the gang. Two fixture sizes were used, one accomodated ten specimens and the other twelve. A schedule number was unique to an autoclave run (except where some Schedule 40 and 50 gangs were simultaneously cured). Specimen numbering on a gang was typically 1 to 12, 21 to 32, 41 to 52, etc. Each complete identification included the schedule number and consecutive gang number; e.g., 53-1, 53-2, - - - 53-12 would all have come from the same gang. Specimens 53-21 to 53-32 would have been bonded on another fixture, but cured in the same autoclave run as 53-1 to 53-12. This arrangement allows comparison of like specimens in a gang. Thus, specimens with a -4 (e.g., -4, -24, -44, -64, etc.) would be in the same relative positions in the respective gangs.

Effect of Cutting on Specimen Temperature:

To satisfy questions on whether the cutting procedure might adversely raise the part temperature, the following experiment was performed. Two pieces of titanium were bonded together with an epoxy adhesive. Four thermocouples were imbedded within the bond line, spaced about 0.5 inches apart (Figure 4). The fused tips of the thermocouples were positioned 0.025, 0.05, 0.10 and 0.20 inches from the intended saw-cut line. A continuous record was used to monitor the temperatures seen by each

thermocouple as the specimen was cut with the diamond wheel. The cutting rate was approximately 1 inch per minute and a hand held squeeze bottle was used to simulate shop cooling. This cooling water flow was less efficient than that employed on the actual experiment.

The highest temperature recorded was 357°F. This occurred for a brief instant when the saw passed through the fused tip of the No. 1 thermocouple, which was obviously located less than the intended 0.025 inches from the blade path. Otherwise, the temperature at the cut line intersecting the No. 1 thermocouple could readily be maintained below 175°F. The maximum temperature recorded as the saw-cut progressed past the second thermocouple (0.050 inches) was about 140°F and the mean temperature about 120°F. Temperature traces are shown in Figure 5.

The conclusion drawn from this experiment was that the heat generated in cutting specimens with a diamond saw is restricted to within less than 0.1 inch of the cut edge and is no greater than the 350°F cure temperature of the adhesive. This heating should, therefore,cause no chemical damage at the bondline. The effects of thermal gradients at the narrow edge region on crack initiation might be of more significance to subsequent fatigue damage growth. But any study thereof would require far greater rigor and replication of specimens than was possible under this program. Also, one should note that specimen width effects were briefly studied in this program (See Section 7) and that significant evidence indicating static or fatigue variation with width was not observed.

SECTION IV

LOAD SPECTRA

The fatigue spectrum used for this program was based upon wing bending moments during maneuver loads for the F-111 fighter-bomber. Figure 6 shows the cumulative load exceedance for the F-111 spectrum and the comparable spectrum from Mil-A-8866 (May 1960).

The continuous load exceedance curve was divided into discrete load levels (given letter names); thirteen of which (plus one ground load) were used to form the test load histories. Load descriptions corresponding to each discrete level are presented in Table 1.

The flight loads data from which Table 1 was developed are summarized as follows:

Time per mission = 3 hours

Missions per lifetime = 1334

Bending moment at nominal cruise (1g) = 2.1×10^6 in lb

Bending moment at limit condition = 20.8×10^6 in lb

Touch-and-Go bending moment = 0 in lb

Minimum bending moment for ground-air-ground = 0.9×10^6 in lb

Test loads were developed in the following manner:

a. Definitions:

Y = bending moment (10^6 in lb)

ΔY = Y-Y (1g) = Y - 2.1 = incremental bending moment (10^6 in lb)

P^B_{UT} = 'B' allowable reduced from static tests of joint (lb)

P^B_{LT} = limit allowable matched to Y (limit) = 2/3 P^B_{UT} (lb)

$$P = \text{test load} = \frac{P^B_{LT}\ Y}{20.8} \quad \text{(lb)}$$

$$\Delta P = P - P\ (1g) = \frac{P^B_{LT}\ \Delta Y}{20.8} \quad \text{(lb)}$$

b. After determination of P_{LT}^{B} from static tests of both the Schedule 40 and Schedule 50 specimens, P was set equal to 200Y; where the constant, 200, was obtained by rounding 195.5 (the actual value of P_{LT}^{B}÷20.8). This produced a condition where the cyclic test limit load was 4160 lb, compared to the 'B' allowable static limit strength, P_{LT}^{B}, of 4060 lb. Proof loads were set equal to 4060 lb.

Select-Random Load Spectrum:

The major portion of the test program involved an engineered or Select-Random load history. This simulated flight history was composed of a repeating pattern of 100 missions. The load sequence in each mission was designed to distribute the moderate and high loads and to group the more frequent lower loads in blocks of high frequency and constant amplitude. This spectrum was derived (a) to allow loads to be easily truncated (i.e., eliminated) with equipment at hand during the beginning of the program, (b) to reduce test times by increasing the application frequency of low amplitude/high occurrence loads, and (c) to assure that each specimen saw an identical test spectrum. Figure 7 shows a typical segment of the Select-Random history, and Table 1 indicates the relationship between load frequency and amplitude.

Each mission had a similar recurrence of the low amplitude loads. Moderate amplitude loads were singularly placed between the blocked lower amplitude loads. Loads occurring less than once per mission were distributed throughout each 100 mission sequence. For example, a load occurring at a frequency of 0.1 per mission would be placed at the same position in missions 10, 20, 30, . . . 90, and 100. The maximum load (1 level/.02 occurrences per mission) was placed near the end of missions 50 and 100.

The sequence of 100 missions was identically repeated, and therefore, formed the basic load pattern that was programmed. Loads that could not be placed in a repeating pattern within the 100 mission group were arbitrarily placed. Individual load levels were readily omitted from the baseline spectrum as required for spectrum truncation.

The 100 mission baseline sequence and truncated sequences were programmed on punched paper tape using a conventional ITI keyboard. The form or profile of each cycle was a straight ramp with a flattened hold at the load peak. This information form was subsequently converted to analog signals on magnetic tape which took the form shown in Figure 7. The analog tapes were used to control a 200 KIP servo-hydraulic test system (MTS), having hydraulic specimen grips. Maximum amplitudes were adjusted to correspond to the required stress levels for the 1/2 inch and 1 inch wide specimens. The inertia of the test equipment tended to round the sharp corners of the programmed load signals, as actually sensed by the specimens.

Random Generation Load Spectrum:

A secondary load history was formed from computerized random selection of the thirteen flight load levels about the 1g condition, at a constant frequency for each load. This load history was run at two frequencies, 1/2 Hz and 8 Hz, for comparison with the Select-Random spectrum on a limited number of Schedule 50 specimens. To increase realism, missions were simulated by including a ground-load (S-level) after every 133d load (See Table 1). A typical load trace is shown in Figure 8.

The random load history was generated, using a PDP-11 minicomputer, by the following steps:

(a) Construct a probability table for each load level (e.g., level G probability was 0.25÷132.97, as derived from Table 1).

(b) Sum the individual probabilities and create a summation table of integers; each load level is now associated with a range of consecutive integers in the table.

(c) Call on a random number generator to produce a number between 1 and the largest number in the summation table. Match that number to each range to determine the load level.

(d) After each random sequence of 132 loads, apply an S-level ground load.

All flight load peaks (positive and negative) were fit to a 120 point half-sine shape. The prolonged ground load had an 80 point hold at the S-level in addition to the 120 point sine shape.

The minicomputer was directly used to run the 200 KIP MTS test system. Each specimen load history started at the same random number. Thus, all specimens subject to the Random Generation load spectrum saw the same load sequencing to failure. A timer within the computer was used to control test frequency.

SECTION V

TEST PLAN

Schedule 50 Tests:

The Schedule 50 specimens (± 45° surface plys) were to determine the effects of the following variables on specimen endurance (i.e., cycles or missions to failure): high load elimination, low load elimination (truncation), Random Generation vs. Select-Random loading, and load frequency. In the elimination or truncation tests, the complete Select-Random spectrum, including all load levels (A to I, P, Q, R, S, T), was used as the baseline. The fatigue lives of Schedule 50 specimens tested with various levels truncated were compared to this baseline. The complete Select-Random spectrum was also used for comparison to the Random Generation spectra, which also contained all load levels. Residual tests of the 3/4 inch joints were also conducted using the Schedule 50 specimens.

Schedule 40 Tests:

The test plan for the Schedule 40 specimens was originally conceived to compare the endurance of these specimens, 0° fibers on the bonded surfaces, to that of the Schedule 50 specimens. The Schedule 50 tests were conducted prior to the Schedule 40 tests. The first Schedule 40 test point demonstrated an extensive endurance. Comparably long endurances were also observed in the initial tests conducted by the University of Dayton Research Institute and ultimately reported in Reference 5. The availability of test equipment precluded continued testing at the load levels of the baseline Select-Random load spectrum. To effect a practical test program, a plan was developed to (a) increase the test stress levels to yield comparable endurances to the Schedule 50

specimens, (b) investigate the sensitivity of fatigue life or endurance to the stress level, and (c) determine the effects of proof testing on endurance. For each series of these tests, all the load levels in the baseline Select-Random spectrum were multiplied by a common factor (Table 7); i.e., the average stresses over the bond line were increased proportionally.

General Procedures:

Static tests were performed on specimens of each group (Schedules 40 and 50) to determine limit loads, batch effects, and to assess any change in strength with age in an air-conditioned environment (72 $\pm$ 2°F 55% nominal relative humidity). The effects of specimen width were also determined from static tests on the 1 inch wide and 1/2 inch wide specimens.

Prior to fatigue testing, each Schedule 50 specimen was statically proof tested at .05 inches per minute (ipm) to 4060 lb, the limit allowable (P^{B}_{LT}). It should be noted that the I level load of 4220 lb is 104% of the proof load. Schedule 40 specimens were similarly proofed to 4060 lb, except as noted in the proof-test-effects tests.

A clamp was placed over the aluminum spacer of the Schedule 50 coupons to keep the failure in the 1/2 inch lap from propagating to the 3/4 inch joint (by impulse or a prying action - a problem determined from preliminary tests). These fatigue-broken specimens were subsequently statically tested to failure (at .05 ipm crosshead speed) to determine the residual strength of the unfailed 3/4 inch joint.

The specimen clamp was moved to cover the 3/4 inch joint during the Schedule 40 tests (conducted after the Schedule 50 tests). This was done to constrain the fatigue failure to the 1/2 inch lap after it was noted in Reference 5 that the large scatter in endurance and the damage growth characteristics could produce fatigue failures in the 3/4 inch joint with great frequency; thereby, effectively aborting a test. Thus, the Schedule 40 tests did not include residual testing of the 3/4 inch unbroken member of the joint pair.

SECTION VI

EXPERIMENTAL RESULTS

Static Tests:

Table 2 summarizes all static tensile tests conducted in the program. Individual data points are compiled in Table 3. Results of the tests conducted in October 1972 for both Schedule 40 and 50 specimens were used to determine the mean ultimate strength and reduced allowable for static ultimate (B-allowable). The six Schedule 50 tests (45° plies on the faying surface) had a mean strength of 6767 lb, which was 3% greater than the Schedule 40 mean strength of 6583 lb. Both groups of data showed a coefficient of variation of 4%. The mean value for all twelve specimens was 6675 lb, which reduced to a B-allowable of P^{B}_{UT}=6089 lb. This value was used as the basis for proof and fatigue load generation.

Effect of Specimen Width:

The specimen width was not rigorously investigated in this program. Nevertheless, from the Schedule 50 data shown in Table 2, the stress capacity of 1/2 inch wide specimens does not appear to have been degraded from edge effects, compared to the 1 inch wide specimens.

Effect of Preload and Fracture Impulse:

Static tensile tests were conducted in September 1973 on four whole specimens, with failure in the 1/2 inch lap followed by a test to failure in the 3/4 inch lap (Table 3). The specimens were clamped over the aluminum spacer to prevent gross failure from propagating

from the 1/2 inch lap into the 3/4 inch lap. The average remaining strength in the larger lap of these specimens 9040 lb was only 2% lower than the average for the four specimens that were not previously loaded to failure in their smaller joint (where the average strength was 9200 lb in these 3/4 inch joints). Thus, evidence from these static tests does not indicate that a contained rupture in the 1/2 inch lap significantly weakened the 3/4 inch lap. One should note, however, that the significance of the residual strength of these eight specimens was reduced by three failures in the boron-epoxy adherend. One might also conclude that loading these bonded joints to about 75% of their ultimate strength will not greatly affect their ultimate strength on a subsequent load to failure. These conclusions bear on the inferences to be drawn from the residual strength tests of this program.

Effect of Age:

From Table 2, data on 1 inch wide specimens tested in September 1973 and November 1974 indicate only a slight drop (1 to 2%) in strength with age on both Schedule 40 and 50 specimens. Tests on 1/2 inch wide specimens showed no decrease in strength with age from 1974 to 1976. Thus, it appears that the specimens were not significantly weakened with respect to room temperature test by aging for one or two years in the air conditioned room where they were stored at room temperature and approximately 55% relative humidity.

Residual Strength Tests-3/4 Inch Joints:

The 3/4 inch lap joints of the Schedule 50 specimens were pulled to failure after initial fatigue in the 1/2 inch laps of the joint. Population means ($\bar{X}$) and coefficients of variation (variance ÷ mean) are shown in Table 4 for the groups of data points. The residual strength for specimen 52-8 was censored since this failure load was less than the spectrum loads on the whole joint just before and at failure. Thus, the 3/4 inch joint must have been severely damaged by the failure of the 1/2 inch joint. Possibly, the clamp used on the specimen was improperly torqued, or the fracture impulse might not always be localized by a clamp. The two other low residual strength specimens, 53-63 and 52-10, may also be suspect with their strength reduction being caused primarily by the 1/2 inch lap fracture, and not the cumulative damage of the test loads. These two loads were not censored. However, for comparison, statistics are shown in Table 4 for data which omits the suspect loads. Note that the data indicate coefficients of variation of 5% or less, and that omitting the two suspect loads maintains this characteristic. Also, the initial static strength data for the specimens (Tables 1 and 2) show comparable coefficients of variation.

The residual strengths were compared to the two groups of initial static strengths for the 3/4 inch joints. This comparison was after both the spectrum testing and constant amplitude tests (Table 4). The residual strengths were lower than the initial strengths, with the mean strength for the weakest group (constant amplitude/P_{max}=2620 lb) being 5% less than the average of the initial static strengths (9120 lb).

Effects of Surface Ply Orientation:

The endurance of the joints with 0° plies on the faying surfaces (Schedule 40) was found to be substantially greater than the joints with 45° plies on the surface (Schedule 50). This is shown for the baseline spectrum (P_I=4220 lb) for Schedule 50 and the single data point (43-3) for Schedule 40, which had about 5 times the life to failure. Also the data from Specimen 42-29 (4.20 lifetimes) helps to substantiate this observation. As further shown in Figure 9, the Schedule 40 specimens can accommodate 30% greater stress levels than the Schedule 50 specimens and achieve an endurance between one and two lifetimes.

Comparison of Data to University of Dayton Research Institute Results:

Figure 9 also presents curves obtained from Reference 5 for 16 ply specimens with layups virtually equivalent to the Schedule 40 specimens. The specimens of Reference 5 were $[0/\pm45/0_2/\mp45/0]_S$ as compared to the $[0/\pm45/0]_{2S}$ design in Schedule 40. The low modulus adhesive used in Reference 5, Hysol EA-9601, differs from EA-951 by being cured at 250F (EA-951 is cured at 350F). Although both adhesives were supposed to be supported films, scanning electron microscope analysis of the Schedule 40 (and Schedule 50) joints did not reveal a fibrous support for the adhesive film. Thus, the EA-951 used by the specimen fabricator must have been received in its unsupported form. Also, room temperature strength of the EA-951 is greater than the EA-9601 (7250 psi vs. 5300 psi, respectively, for coupon tensile shear over 1/2 inch lap, as per manufacturer's specifications A5-230 and A5-234).

The initial or static strengths for both the Schedule 40 and Schedule 50 specimens are 20% higher than the initial strengths for the specimens bonded with EA-9601 in Reference 5. Endurance curves similarly vary for specimens with 0° plies on the faying surfaces (Figure 9). Further relations are discussed in the forthcoming paragraphs.

Effects of Stress Level on Endurance and Residual Strength:

In Reference 5 it was noted that the drop in endurance becomes very rapid as the highest load of the general test stress is increased above 80% of the static ultimate strength; that is, where the magnitude of each spectrum load is multiplied by a constant (K). The knee of the Schedule 40 curve in Figure 9 is where KP_I is also approximately 80% of the static tensile strength. This compares reasonably with the data for EA-9601, also shown in Figure 9.

The very nature of a fatigue test is that failure occurs when the residual strength is degraded below the failing load. Endurance curves as presented in Figure 9 can be considered as a series of limited residual strength tests that are discontinued at the peak loads for each cycle. Most specimens failed during one of the two highest load cycles in the load spectrum (Levels H and I, Tables 4 and 6). Thus, one might consider the endurance curves as a band of residual strength points with a vertical spread between P_I and P_H. The curves of Figure 9 tend to become horizontal going towards the left. This indicates that a drop in residual strength to 80-90% of the initial strength occurs early in the test history. This is in the region where endurance is below 1 lifetime and highly sensitive to general stress levels. The

rapid drop in residual strength is probably due to damage caused by the peak loads rather than cumulative damage from the lower level loads. Support for this conclusion can be obtained from the effects of the proof test experiments in the next section.

Effects of Proof Test on Endurance and Static Strength:

Sixteen one inch wide and six 1/2 inch wide specimens from the Schedule 40 population formed a data base for estimating the effects of proof load on specimen performance. The proof test was conducted prior to fatigue testing in the same manner as that conducted during the Schedule 50 portion of this program. This involved a constant cross-head rate of 0.05 ipm to one of the proof loads, 6000 lb, 5500 lb, 4060 lb, or zero for the one inch wide specimens. The set of 1/2 inch wide specimens was proofed to 2030 lb or zero in a similar manner. The loads were relieved at 0.05 ipm.

The effects of spectrum intensity and proof load on endurance are summarized in Table 7. Further tabulation of the proof load data and the effects of one long lived specimen on mean test data are shown in Table 8. This high endurance point (specimen 43-29) is considered to be representative of the low probability 'tail' of the distribution curve for its respective data group since it exceeds all data, even for less severe proof loads, and this endurance is significantly greater than that for all thirty Schedule 40 tests where KP_I is greater than 5000 lb (Table 6). Thus, it is not representative of the central tendency of its data group.

The proof test data is plotted in Figure 10 for the 1 inch wide specimens. From the results for the one inch wide specimens there is evidence that a proof test at 4060 lb or 62% of the reduced ultimate strength allowable will damage the joints (an endurance reduction to 64% of the unproofed mean data). Also the data in Table 7 for the two 1/2 inch wide joints tested at KP_I=2750 lb, where proof tests were to 62% of the ultimate allowable, indicate a significant reduction in endurance to 61% of the unproofed joints.

Thus, it appears that proof testing of these joints at or near their static limit strength will reduce endurance - even for a flight load spectrum having comparable or higher loads in it. This would indicate that the slowly applied (.05 ipm) high initial load prior to the application of numerous low amplitude "working in" loads may be significantly more damaging than a load of comparable or even higher magnitude encountered later in the test history. As an area of future study, the effects of a proof load near static limit should be determined for joints tested at a load spectrum designed for long life; for example at the Baseline Spectrum of this program (which would not be multiplied by factor K to achieve shorter test times).

At a proof test of 5500 lb (1% greater than the maximum fatigue load, KP_I) the data (excluding specimen 43-29) indicate that a proof test at 5500 lb causes a reduced endurance of 54% of specimens

not proof tested. This proof-load is 90% of the reduced (B allowable) ultimate strength. In Reference 5 a comparable initial load of 86% ultimate produced an endurance that was 53% of the nonproofed data.

Schedule 50 Endurance-Baseline Spectrum:

The results of Schedule 50 fatigue tests are listed in Table 4 and summarized in Table 5. Baseline data indicate a reduced endurance in the specimens from Batch 52, compared to Batch 53. However, a weakness or difference in endurance was not apparent between the two batches in the various truncation tests. In fact, the specimens from Batch 52 tend to average greater endurance than the Batch 53 specimens in both the truncation and constant amplitude tests. Thus, the data for the baseline endurance of specimens 52-3, 52-8, 52-23, and 52-28 (which was taken during the start up phase of the fatigue testing) may be suspect.

Schedule 50 Endurance-Random Spectrum:

The average specimen endurances under randomly applied loads at constant frequencies are indicated in Table 5. Since each of the eight specimens was from Batch 53, the endurances are compared to the baseline endurance of 1.26 lifetimes. The random endurances are 36% and 38% of the endurance for the baseline tests, for the 1/2 Hz and 8 Hz, respectively. One should note that the range of frequency in these tests is close to the maximum and minimum frequencies of the baseline spectrum (10 Hz and 1/4 Hz, respectively). The 4% reduction in lifetime at 1/2 Hz compared to that at 8 Hz may be attributed to creep effects, but is probably more related to experimental scatter.

These data show that the random loading is more damaging than blocked or quasi-blocked loading. Also, the validity of this comparison is supported by the fact that loads in both spectra in the program started from the same condition (1 g). That is, the load ranges were the same. In the case at hand the major blocking was with the low amplitude loads since the higher amplitude loads were applied reasonably dispersed (Figure 7). Actually, loads of magnitudes A and to a lesser extent B often occur in short blocks, even in random selection, due to their large number of occurrences relative to the other discrete loads (Figure 8).

Load Truncation:

From Table 5 the effects of low and high magnitude load elimination or truncation can readily be appreciated. The low loads are often excluded in fatigue testing of metal structures to afford test economics. High magnitude loads may be excluded to eliminate the complexities of simulating the chance occurrence of very remotely occurring loads.

Low Load Truncation:

A 1g incremental bending moment about the 1g cruise condition is typically taken as the cut-off or lower truncation for metal fatigue tests. With a 1g load of 420 lb for this study (Table 1), the A level test load is 1.4g above the 1g cruise. This level was truncated, as were both the A and B levels together. Additional truncation of load levels would eventually lead to the high endurance limit indicated in Figure 11, where the constant amplitude endurance at load level I would be approximately 190 lifetimes, based on reversed constant amplitude

data and 285 lifetimes for non-reversed loading. These somewhat academic limits were derived by dividing the cycles to failure load level I (4220 lb), found in Figure 12, by 26.68, which is the number of occurrences of P_I per lifetime. Similarly, were additional load levels applied to the lower end of the test spectrum (e.g., the M level of Table 1), one would expect the endurance curve to trail off to some average lifetime below the 1.26 lifetimes found for the baseline load spectrum.

The slope of the curve for these data in Figure 11 indicates that careful attention must be given to the selection of a lower truncation limit for a given test program. The + 1g level about the cruise condition should not arbitrarily be used as a lower truncation even though it may correspond to only 20% of the spectrum limit load.

In Reference 6 additional low amplitude loads between 30% and 50% of the design limit load were added to the baseline spectrum of the study. A marked decrease in endurance (73%) was found. Although these data on bonded step-lap joints do not directly support conclusions in the present study, they do further indicate that low level truncation, in various forms, is of great significance. On the other hand, data from Reference 5 indicated little decrease in endurance where levels A and B were truncated. An explanation for these divergences of results is not apparent. One might explain the data conflict around the fact that the joints tested in this latter reference were not comparable to

the Schedule 50 joints. That is, the joints in Reference 5 had 0° plies on the faying surfaces, not ±45° plies. On the other hand, the step-lap designs of Reference 6 had 0° plies on faying surfaces and they were greatly affected by low amplitude loads.

High Load Elimination:

Load Levels removed from the baseline spectrum for the high load elimination did not include the removal of the maximum load (I level). Thus, in effect, these tests involved a limited residual strength test every 50 missions.

The marked increase in endurance with the elimination of high loads is plotted in Figure 11. Note that the eliminated loads (F, G, and H) each occur less than one time per mission (Table 1), and that the G-level load is 84% of the design limit load.

Constant Amplitude Fatigue - Schedule 50:

Constant amplitude data were obtained on the Schedule 50 specimens; both to compare any effects on the mode of failure to random load fatigue, and to investigate the suitability of this type of data to fatigue life prediction. An inclusive constant-life diagram, mapping a S-N endurance for ranges of minimum load (P_{min}) and maximum load (P_{max}) was beyond the scope and intent of this program. Also, numerous studies (e.g., References 1 and 4) have shown that a Miner's Rule analysis of simulated-flight or random loading will lead to over optimistic results in predicting the endurance of bonded composite joints. Therefore, the basis of this phase of the study was to (a) obtain a constant amplitude

(S-N) curve with reversed loading, (b) obtain a tension-tension constant amplitude curve based upon a minimum load (P_{min}) taken as the lg flight condition (Table 1), and (c) compare failure modes and estimate endurance using these two curves.

Data from the reversed load and the tension-tension tests are summarized in Table 4 and displayed in Figure 12. One data point (specimen 51-6) was censored based upon irregular proof test performance that indicated a partial failure during the proof. The reversed load tests were arbitrarily conducted at what was considered to be a severe amount of compression compared to that encountered in the baseline spectrum. That is, the two conditions tested for R=-0.2 had minimum loads of -812 lb and -524 lb, respectively. These compare to the two lowest loads in the baseline spectrum, -980 lb and -580 lb, which only occur twice and 13 times, respectively, per one hundred missions. Also, the ratio of compressive loads, zero load crossings to positive loads (peaks and valleys), is only 0.038 in the baseline spectrum.

As expected, load reversal decreased specimen life from the all-tension tests. The reduction at P_{max}=4060 lb was to 67% of the all-tension endurance, and at P_{max}=3020 lb the reversed stress endurance was only 22% of that for the tension-tension cycles.

Miner's Rule Analysis - Schedule 50:

The most damaging constant amplitude S-N curve of Figure 12 was used to obtain constant amplitude cycles-to-failure (N_i) at each of the load levels (i-A to I, inclusive). These values and the number

of peaks for each load level occuring per lifetime in the load spectrum (Table 1) were combined to obtain linear damage estimates. Table 9 indicates the results for the classical $\Sigma(n_i/N_i)$ of Miner's Theory. The right hand columns show the damage at failure for the various Schedule 50 spectra tested. As seen, the cumulative damage by Miner's Rule for the baseline spectrum only attained 6.56% at failure (compared to the 100% required by Miner). Similarly, damage estimates for the truncated spectra would have been highly unconservative were Miner's Rule used. The inappropriatness of linear damage estimation becomes even greater where more random load simulation is used, and where more rigorous constant amplitude data shift the S-N curve to the right (Figure 12).

A method to use Miner's Rule or linear damage analysis to develop an understanding of the effects and interaction of each of the load levels is not readily apparent. Further testing, wherein the successive truncation of loads is performed might yield a data base which could increase our understanding of the importance of the interactions of the high loads on the damage caused by the lower loads. Nonetheless, there appears to be no substitution for good flight-by-flight simulated testing in the structural design and verification process.

SECTION VII

FAILURE MODE STUDY

General Observations:

The failed specimens were catalogued by test type (e.g., static, random fatigue, constant amplitude fatigue), failure pattern, failure mode and approximate percent thereof over the fracture plane, and the relationship of failure to the location of scrim material. Figure 13 describes the general failure modes and patterns observed. Most modes could be differentiated. However, the distinction between cohesive failure within the adhesive, and adhesive failure at an adherend was sometimes obscure, where a very thin film of adhesive might remain on the adherend. Figure 14 shows the ruptured surfaces of a typical Schedule 50 fatigue-failed specimen, 52-38. Two modes of failure predominate; viz., Mode B shear along the bare boron fibers and the torn (tensile failed) regions in the $\pm 45^{o}$ plys at Edge T (Mode D).

A scanning electron microscope (SEM) was used to study the failure surfaces and observe fracture patterns. Figure 15 includes four pictures of failure areas on the titanium strap of a fatigued specimen (53-31) taken at 150X. Figure 15A is a boundary between a B-type failure mode and a cohesive failure (Mode C). The bundle of fine fibers is a yarn of scrim (104 style glass fabric.)

Figure 15B was taken in the center of a large area of cohesive failure in the adhesive (Mode C). Figure 15C shows an area where the adhesive failed on the titanium surface (Mode A_T). To the naked eye this area had a dull appearance and it was suspected that a thin layer of adhesive might have remained on the surface. A shiny area where the titanium was scraped when prying the specimen apart was examined to compare with Figure 15C. This is shown in Figure 15D where the sanding pattern from the prebond surface treatment is clearly shown. Pictures of each of these areas taken at 15X are shown in Figure 16.

Figure 17 shows a 15X view along Edge T of the central adherend of specimen 53-31 where bare boron filaments (Mode B) meet $\pm 45^{\circ}$ filaments (Mode D). Note the 0/90 degree oriented woven scrim, and a triangular patch of cohesive failure in the adhesive (lower left hand corner). Figure 18 shows a typical area at 15X, 75X, and 150X. Note that in low magnification the bare boron filaments appear concave, whereas at higher magnification the actual surface features of the boron are seen. A scrim filament appears in the center of the 150X picture. The adhesive is seen to not have a woven carrier, and scattered chunks of laminate resin are seen on the boron filaments.

Summary of Failure Modes:

One or two characteristic failures were observed for each test and specimen type. Table 10 summarizes the typical failure modes by percent and pattern over the boron epoxy failure surfaces. In studying the table it should be recalled that the nonscrim surface of the central adherend did not have a balance scrim ply over the outside or surface ply of boron. Also, the last column defines the failure pattern on the surface considered to fail first. Schematics of the specimen layers are shown in Figure 19. To understand the format of Table 10 consider the Schedule 40 fatigue tests. Two modes were characteristic:

(a) Sixty-five percent of the specimens had a predominantly Pattern 40-2 failure on the scrim side where the Mode B failure varied from 50 to 80 percent of the area. The reverse side showed a wide range of failure with the amount of bare 0^{o} filament ranging from 10 to 90 percent. Areas that were not Mode B (on both failed surfaces) were predominantly cohesive failures (Mode C).

(b) Another group of specimens, 35 percent of the total, failed on the scrim side along the outermost 0^{o} boron ply in Mode 40-1T, with 80 to 99 percent of the area showing Mode B. The sides failing secondarily had between 60 and 90 percent Mode B failures over the fracture surface. The remaining fractures of these surfaces were also predominantly cohesive in the adhesive.

Apparent Side for First Failure/Basis for Selection:

Test apparatus suitable for detecting the specimen side or faying surface of the central adherend to first rupture was not developed or employed in this program. Thus, the catalogued data in Table 10 that summarize or state the predominant side for first failure are somewhat subjective in nature. The selection of the apparent surface for first failure in the double lap joints was strongly based upon the following rationale dealing with type of failure and amount of failure:

(a) A uniform failure of Mode B over a large area of one side of the boron adherend indicated first failure, where the reverse surface had a partial cohesive failure, a torn or mixed mode appearance, or a lesser amount of B failure.

(b) The second surface to fail has been thrown into single-lap-type peel and impulse loads. It, therefore will tend to have greater clevage and more nonuniform failure, often penetrating into the inner plies.

(c) A major area of adhesive failure (A_B or A_T) indicated a side for first fracture.

Each of these assumptions can be partially supported by deductions relating modes of failure to internal stresses. Also, a logical analysis relating the various tests, specimen designs and hypothesized failures was conducted in this study to assure all failure hypotheses were consistent with each other. Discussion of such are included in

subsequent paragraphs. But, regardless of its complete validity, the rationale presents a consistent set of criteria for comparing failure to the scrim or nonscrim sides of the specimens. This comparison was useful in determining whether the application of scrim is an important factor in joint design and endurance.

Stress Patterns:

From References 3 and 4 the stress pictures for these joints in tension would be as shown in Figure 19. Shear stresses in the adhesive and central adherend are greater in the region near the end of the titanium straps (Edge T) as compared to near the end of the central adherend (Edge F) since the stiffness of the outer adherend is greater than that for the boron/epoxy. Also, the peel stresses reach a positive peak at this same edge. Thus, one would expect that the mode or modes of failure might normally originate in the adhesive or in the boron laminate near the edge of the titanium strap. After one side of the specimen fails, the specimen behaves as a single-lap joint with very high peel and shear stresses at both edges of the bonded area.

In Reference 4, SEM pictures were taken to establish the difference between a peel and shear mode of failure along an exposed boron/epoxy ply. Also, high magnification was employed to observe the resin cracks and relate them to the directions of principal stresses.

Numerous observations along the Mode B failure surfaces on the boron/epoxy adherends, of representative specimens from each of the test groups and schedules, were taken. Pictures were taken near Edges T and F and at the mid-lap. In all cases where a Mode B failure existed, shear fractures were observed in the resin areas between the boron filaments. Figure 20, taken perpendicular to the ply planform, shows the interfilament tensile surfaces along planes inclined to the direction of load. The slope of these small surfaces with respect to the specimen tab or load direction can be better seen by observing the residue on the titanium strap that shears from the boron/epoxy adherend. Figure 21 presents an angle view of the interfilament region. Figure 22 shows the view of the Figure 21 area taken perpendicular to the surface. These sawtoothed cracks should be perpendicular to the direction of principal stress, and indicate that a static failure occurred. The angle is seen to be 30^{o} or less and indicates that both shear and peel forces are operative. Similar patterns were observed on fatigued specimens. That is, 'pup tent' crack patterns, indicating reversed stresses during crack growth, were not observed. This was contrary to data in Reference 4 where fatigue failure under reversed loading was shown to occur in the laminating resin (Mode B) by toothed pattern where both sides of the tooth were sloped, indicating principal stress reversal. Unidirectional or static shear fracture patterns from this reference had sawtoothed patterns comparable to Figure 21.

Failure Mode for Static Tests/Schedule 40:

Approximately 50% of the 1 inch wide specimens and two of the three 1/2 inch wide specimens failed with the scrim side having Pattern 40-1T. The T indicates that the boron shear failure butted right up to Edge T (Figure 23A). Only one specimen failed with this pattern on the nonscrim side. Two out of the nine 1 inch wide specimens failed with 80% C and almost 100% A_B, respectively, on the scrim side. The remaining specimens failed in Mode 40-2 on the scrim side, with less than 20% Mode B on this surface (Figure 23B).

The reverse side (nonscrim) for these static specimens was mostly a mixed mode of B, C, and A_B (Pattern 40-3) with the Mode C generally occurring along Edge T, and with A_B near Edge F (Figure 23C). Only one specimen out of the 12 tested had a rupture down to the next lower 0^o ply, and only one had a narrow strip (20%) of Mode B along Edge T.

From the failure criteria previously outlined, the most probable first surface to fail was the scrim side, for the specimens having Pattern 40-1T. Shear between the 0^o boron and its scrim occurred in the most stressed area (shear and peel), as in Figure 19 and seems to be the likely failure initiator. The one ragged interply fracture was on the nonscrim side of a specimen having Pattern 40-2 on its scrim side. Also, the remaining patterns on the nonscrim side for these specimens were comparable to the nonscrim sides of the Pattern 40-1T specimens. This tends to indicate that these specimens also failed on the scrim side. However, the small amount of Mode B and its location away from Edge T makes it likely that the rupture initiated within the adhesive.

Failure Mode for Fatigue Tests/Schedule 40:

Of the one inch wide specimens, 65% failed with Pattern 40-2 on the scrim side, where the oval B area was typically 60% of the total faying area, and often reached Edge T (Figure 24A). The remaining specimens failed in Pattern 40-1T on the scrim side. Here, the B area was usually 80 to 99% of the total, with scattered broken 0° filaments (Figure 24B). The nonscrim side for the 1 inch specimens generally failed in a mixed and rather ragged mode with 50% showing interply failure to lower plies (Figure 24C). Thirty percent of the nonscrim surfaces were of Pattern 40-1 (Figure 24D), some almost 100% B failure. Many failure surfaces had 10 to 20% Mode C failure along Edge T; and generally a narrow cohesive/adhesive zone at Edge F, even where most of the failure surface was Mode B.

Figure 25 shows failure surfaces of the one fatigue test for Schedule 40 that was cycled past 7 lifetimes and failed in its 3/4 inch lap. The pattern of the larger lap shows a high percentage of Mode B. This indicates that fatigue damage occurred, a conclusion supported by the larger fraction of Mode B compared to static tests.

The 1/2 inch wide fatigue specimens mostly failed with Pattern 40-1T on the scrim side, where the B area ranged from 80 to 95% of the faying surface. The reverse surface had some mixed modes, but with 60% showing Pattern 40-1. These latter specimens typically had most of the cohesive (C) failure along Edge T.

SEM examination of the failed B surfaces showed a saw-toothed pattern in the laminating resin along the B failure plane (Figure 20). This pattern indicated unidirectional shear at failure with no indication of cyclic damage growth. That is, the pattern was similar to that for the static specimens. An attempt to detect stress reversal and fatigue growth was made by observing the valleys on the matching sides to the bare boron fibers of the central adherend; i.e., by magnifying the shear surfaces on the titanium straps. No 'pup tent' crack pattern was noted.

Discussion of Schedule 40 Results:

A comparison was made of the static failure surfaces to the fatigue failures for Schedule 40 specimens. The following differences were noted:

(a) Fatigued specimens have a greater amount of Mode B on the scrim side, both for Pattern 40-2 and 40-1. Also the nonscrim side for the fatigued specimens had more Mode B surface area. Thus, fatigue must be weakening the shear between the 0^{o} fibers and the laminating resin. This weakening is present for both the 1/2 inch joints and the 3/4 inch joint tested. The damage apparently weakens the 3/4 inch joint at a rapid rate, thus creating the situation where many 3/4 inch joints were failing before the 1/2 inch joint (as in Reference 5).

(b) The fatigued specimens had a greater tendency for interply failure down to the next 0^{o} ply on the nonscrim side, which is hypothesized as the second side to fail.

(c) Pattern 40-2 failure may be caused first by cohesive failure in the adhesive in the region of the high shear and peel (edges and sides), followed by shear along the boron filaments. Support for this comes from the SEM pattern of a unidirectional failure stress along the 0^{o} layer. However, a valid rationale explaining the greater succeptability for cohesive failure in the adherend on the scrim side is not apparent - unless one assumes that the added thickness of low modules scrim and resin allows the adhesive to strain more.

(d) Pattern 40-1 with Mode B along Edge F was not observed. This indicates that fatigue damage did not start at the boron interfaces in the high shear area adjacent to Edge F and subsequently cause fracture to move inward, until the shear ultimate of the remaining bond area was reached.

(e) The fatigue specimens failed in Pattern 40-2 at twice the frequency of occurrence as for the static specimens (for the limited samples tested). This, along with the larger percent of Mode B in the central region of the failure pattern may indicate that the cyclic adhesive damage growth was restricted to closer to the specimen edges and sides, and that it progressed at somewhat greater rate than the damage growth in the laminating resin/boron interface along Edge T.

(f) The failures of both the static and fatigue tests where Pattern 40-1 occurred on the scrim side are hypothesized to initiate on the scrim side along Edge T between the $0/90^{o}$ scrim and the outer 0^{o} plies. The Mode B typically progressed to near Edge F where failure changed to cohesive (Mode C) and adhesive (Mode A_B). Often the Mode C failure at Edge F was a narrow transverse strip, in fatigue. This failure type occurred in 50% of the static test failures, except that these had a greater amount of cohesive failure (Figure 23A vs. Figure 24B). The nonscrim side of the fatigue specimen often had B failure from just inside Edge F to near Edge T, where cohesive failure occurred. The nonscrim surfaces from the static tests were mostly Pattern 40-3.

(g) The tendency for a sharp failure along Edge T on the first surface to fail is predictable since this area has both high shear and normal (peel) stresses. The frequently observed Pattern 40-3 for the second failure surface (nonscrim) where cohesive failure occurs along Edge T (as opposed to the sharp type B failure on the first surface to fail) may indicate the effect of greater peel as the joint changes to a single lap.

(h) A possible scenario for these failures can be hypothesized with the aid of Figure 26. First failure is assumed to initiate along Edge T (Point 1) with a fracture of the scrim and surrounding resin. Next static shear propagates along the 0^{o} boron until the specimen cocks enough to cause peel in the adhesive (Point 2). High peel on the nonscrim side causes some cohesive failure in the adhesive

and laminating resin (Point 3), but most failure is Mode B. Finally, a stress picture similar to Point 2 occurs at Point 4. The frequency of this failure sequence on the second side to fail (nonscrim side) was diminished by the greater tendency for ply splitting and mixed mode failure on this severely stressed side.

Failure Mode for Static Tests/Schedule 50:

Six out of the eight 1/2 inch wide specimens failed with the nonscrim side generally showing about 80-90% adhesive failure on the boron/epoxy surface (Mode A_B). Of the other two specimens one failed with 80% A_B on the scrim surface and the other with 50% C/40% A_T. The six similar specimens all had fractured 45^o filaments in a sharp line along Edge T with some of the laminating resin pulled off. Also, in a small number (2) of specimens, clusters of short diagonal fibers near the sides at Edge T pulled out, exposing part of the second (45^o) ply. Fifty percent of the 1 inch wide specimens showed this same mode (A_B) of failure (Figure 27A), which is described as Pattern 50-2. With but one exception, this failure pattern was only found on the nonscrim surface. The other 1 inch wide specimens failed with Pattern 50-1 and over 90% Mode B on the nonscrim surface. These had strengths below the average for Schedule 50. Numerous scattered spaces of pulled out boron fibers were observed on all the Mode B (0^o) surfaces.

Most joints just described failed on the reverse surface to those just described with a ragged and mixed mode down to the first 0^o ply (Figure 27B). The Mode D failure had extensive shear over the second exposed 45^o ply, and Mode B failure was about 60% of the overlap area. Ten to 20% A_T/C failure was often clustered near Edge T on this reversed surface.

Of the two 3/4 inch lap jonts that were statically failed without first failing the 1/2 inch lap side (and did not break in the central

adherend outside the joint), one failed as Pattern 50-2 on the nonscrim side, the other failed with 100% A_B on the scrim side. Both reverse surfaces were Pattern 50-1, with 70-80% Mode B.

The failure patterns on the 3/4 inch lap side of the joints that first statically failed in the 1/2 inch lap were observed. All showed first failure on the nonscrim side with a sharp break along Edge T in the 45^{o} plies, followed by interlaminar shear (Mode B) along 95 and 98% of the overlap area. The reverse side (scrim side) showed a sharp break in the first (surface) 45^{o} ply, with 20% of the record 45^{o} ply remaining as bare boron filaments.

The failure pattern for the 3/4 inch joints that were cycled and statically tested after failure in the 1/2 inch lap of the coupon, was identical to the 1/2 inch lap pattern. These joints first failed on the scrim side, contrary to the patterns of the Schedule 50 static tests. Thus, the reaction of the $0/90^{o}$ scrim to cyclic loading has significantly affected the joint failure mode.

Excepting the 3/4 inch lap joints just discussed, the results of these tests indicate that the predominant first failure was on the nonscrim side and by Pattern 50-2. The sharp failure along Edge T may be due to both high peel and tension in this ply since filaments were seldom sheared out. Had the adhesive bond been stronger, those that failed as Pattern 50-2 probably would have continued to fracture through the two surface 45^{o} plies and ultimately failed as Pattern 50-1 with shear along the first 0^{o} ply; i.e., as did 50% of the 1 inch wide specimens.

In reaching this conclusion on first failure, the following were considered:

(a). The predominant failure on the hypothesized first surface to fail was regular and orderly, with no evidence of prying or high peel. For example, the fracture along Edge T was clean, versus the ragged fracture on the reverse side.

(b) The predominant failure pattern on the hypothesized side for second failure was mixed and ragged.

(c) The second side to fail had an appearance comparable to the assumed side for second failure on the fatigued specimens of this test schedule. Also, the clean break along Edge T of the surface 45^{o} ply was characteristic of the first surface to fail on the fatigued specimens.

Failure Mode for Fatigue Tests/Schedule 50:

The predominant fracture on the scrim side for reversed-load fatigue was Pattern 50-1, with 80-90% B failure. No evidence of reversed stress resin cracking was found along the B fracture plane. The Mode D failure in the $\pm 45^{o}$ surface plies was quite sharp through the plies, and was perpendicular to the load direction. A shear failure initiated in the laminate resin between the first 0^{o} boron filament and the scrim for this layer (oriented 0/90 degrees). This failure was, therefore, on the scrim side of the central adherend under the outer $\pm 45^{o}$ plies. The nonscrim side showed a similar failure with bare boron filaments, but with a lesser amount (45-70%) of the B failure. Figure 27C shows a typical failure. No evidence of peel at or near Edge F was noted from

microscopic examination of either the fractured resin between the boron filaments or on the outer surfaces of the boron filaments. The latter were examined from the fracture residue on the titanium strap.

Those fatigue tests that were conducted without reversed loading (constant amplitude tension-tension loading) showed a similar failure to the baseline and reversed load (tension-compression) constant amplitude tests. However, one exception was that 65% of the tension-tension tests had first failure on the nonscrim side. In this regard, they behaved more like the static tests for this schedule.

Discussion of Schedule 50 Results:

(a) The reversed-load fatigue tests primarily failed with extensive Mode B damage on both faying surfaces. This compares with failure on the nonscrim side for static and tension-tension fatigue tests (Table 10), and with the predominantly adhesive failure of the static specimens. Thus, it is hypothesized that the fatigue process weakened the interface between the 0^{o} boron on the third ply of the scrim side and its 0/90 oriented scrim layer. This led to a shear failure which dumped all load from one titanium adherend into the two top $\pm 45^{o}$ plies. These immediately ruptured in tension. The second surface to fail had a greater percentage of Mode B than the static tests since it too was weakened in the fatigue process.

(b) Failure being primarily on the scrim side of the Schedule 50 specimens implies that scrim oriented at 0/90 to the load direction is more damaging in reversed fatigue than scrim oriented at $\pm 45^{o}$. This

is reasoned from (a) the failure does not occur on the nonscrim side where ±45° scrim mates with the first 0° filaments, and (b) failure did not occur on the scrim side between the 0/90 scrim and the inner side of the second 45° ply. However, the difference in the rate of damage propagation is not great, as evidenced by the relative extents of shear along the two 0° boron planes.

(c) The slightly greater static strength of the Schedule 50 specimens compared to the Schedule 40 specimens may be indicative of the modes of failure. That is, in the Schedule 50 specimens the load along the outermost 0° plane has been reduced by shear lag through the two surface plies. This explains the great propensity for failure in mode A_B along the exterior of the central adherend in these specimens.

(d) The scrim side of the boron/epoxy adherend appears to be stronger than the nonscrim side even where the failure mode is adhesive. This can be explained by reasoning that on the scrim side the 0° scrim filaments strengthen the 45° surface ply over the outer ply on the nonscrim side. This latter ply fails along Edge T where tensile loads are greatest. This local failure may be gradual, and may simply transfer shear into the next 45° ply (which is stiffened by the third (0°) ply) until surface shear reaches the limit of the adhesive. Possibly, the fracture along Edge T may be sudden, thereby creating an impulse stress that exceeds the adhesive limit.

(e) The failure pattern of the constant amplitude, tension-tension tests may be produced by a general fatigue weakening of the resin along the 0° filaments of the third ply on both sides of the central adherend. Concurrently, fatigue failure of the outer 45° plies may be occurring. Thus, ultimate failure may often first initiate in the surface 45° ply, as in the static tests. Were a fatigue mechanism, comparable to the random fatigue tests, the primary cause of damage growth (along the 0° ply), one should suspect a greater amount of Mode B failure on the scrim side than was actually found.

Discussion of Fatigue Failure Modes/Schedule 50 vs. 40:

(a) As reported herein, Schedule 50 reversed-fatigue appears to propagate more readily on the scrim side between the first 0° ply and its 0/90° oriented scrim layer. The Schedule 40 fatigue damage also favors the scrim side, and a similar orientation of scrim and 0° ply occurs along the failure planes (see the section blowups in Figure 19). However, the failure of the Schedule 40 specimens under fatigue may often occur with the adhesive as the weak link (i.e., the 0° boron interface is not weakened as much as it is in the Schedule 50 tests). Also, the Schedule 50 design has an endurance of roughly 20% of the Schedule 40 layup. If one hypothesizes that the rolling action of the 90° scrim threads might induce early fatigue of the adjacent resin on the first 0° plies in Schedule 50 fatigue , then the same reasoning should hold for Schedule 40 fatigue. Here, an increase

in the percent of Mode B compared to static tests was observed, but a significant number of specimens also appeared to initially fail in the adhesive (Mode C). A major difference between the Schedule 50 and 40 designs is that the Schedule 40 failure surface and its $0/90^{o}$ scrim is cushioned in the low modulus adhesive. It, therefore, might be less damaged by the scrim movement on microstrain. Thus, the reduced laminate damage and longer endurance would allow the fatigue degradation of the adhesive to become more significant.

(b) The fatigue failure for both Schedule 40 and Schedule 50 occurs predominantly along the outer surface of the first 0^{o} boron plies. The endurance of the Schedule 50 specimens is substantially less than that for the Schedule 40 specimens. Yet, the shear stress along the 0^{o} failure ply in Schedule 50 should be less than that on the Schedule 40 ply, due to shear lag towards the center of the boron epoxy adherend. Possibly, the rationale given in the preceding paragraph (a) can explain the lower endurance of the Schedule 50 specimens. That is, although the shear stress is slightly less, the more brittle nature of the surrounding laminate resin causes greater micro-stresses along the boron-to-scrim interface in the Schedule 50 specimens.

SECTION VIII

CONCLUSIONS AND RECOMMENDATIONS

1. High occurrence loads having magnitudes near +1g about the mean cruise condition have a substantial effect on the endurance of boron/epoxy-to-titanium (B/Ep-Ti) bonded joints and should not arbitrarily be neglected simply to condense test times and costs. Additional work is required to investigate the effects on cyclic life of tensile and compressive loads in the 1g zone about the mean.

2. The omission of high loads, occurring less than once per mission increased endurance by 500 percent on the joints with ±45 degree plies on the faying surfaces of the composite adherend. The effects of high load truncation on joints optimized for endurance (0 degree surface plies) should be determined.

3. Bonded double lap B/Ep-Ti joints, designed with ±45 degree plies on the faying surfaces (where zero degrees is the main cyclic load direction) had only 20 percent of the endurance of joints designed with the same number and orientations of plies but with 0 degree plies on the surfaces. Both joint types were nearly equal in static strength. The joints with 0 degree surface plies could be stressed 30% higher and still achieve comparable lifetimes to the ±45 degree-surface joints in the 1 to 2 lifetime range. Also, joints designed with a 0 degree ply on the faying surface are expected to exceed 4 lifetimes, under a flight-by-flight test spectrum that truncates negative loads and is based upon matching 'B' allowable static strengths to flight limit loads. Both joint types experienced

a reduction in strength between zero and one lifetime. Data should be developed on the characteristics of these joints between 0 and one lifetime. Also, design information based upon empirical data should be acquired prior to establishing the bond-surface plies for biaxial stress conditions and for hybrid designs.

4. The mode of failure for bonded B/Ep-Ti joints is dependent on the location of the scrim layer for each ply. This layer may augment the static strength of some designs, but tends to weaken high endurance designs if located on the exterior of an adherend. The modes of failure and relative strengths and endurances of joints designed with 0 degree or $\pm$45 degree plies on the faying surfaces are related in part to the scrim location. When pooling static or fatigue data to increase the general population for statistical significance, the mode of failure should be considered as it relates to scrim location. As an area of future study, techniques to orient the scrim at $\pm$45 degrees to the boron fibers may prove advantageous to endurance and could potentially be accomplished either during the manufacture of the prepreg or when adding a balance scrim to the composite laminate. Also, laminate designers could arrange ply stacking such that the scrim does not appear on the exterior. The effects of scrim on static and fatigue strength of hybrid composites (boron, graphite, glass/epoxy) should be explored. A class of hybrid material might be tailored by using various weaves and orientation of glass (or Kevlar and graphite) as the scrim for the boron prepreg. These could be optimized for endurance.

5. Reversed fatigue loading that included both positive and negative loads affected both the mode of failure and the associated cycles to failure. In this program, a decrease of over 30% in constant amplitude endurance was observed when negative loads equal to 20% of the positive loads were applied to each load cycle.

6. A fully random load sequence reduced endurance by a factor of three for the bonded composite joints, compared to a partially random spectrum with constant amplitude or block-load sequencing of the low amplitude loads.

7. The state of damage to a structural member at a given time under fatigue loading is generally theorized to be a function of an initial damage condition and/or damage initiation. As noted in this program and in an associated investigation (Reference 5) for B/Ep-Ti joints designed with 0 degree surface plies, there is a significant probability that a 1/2 inch lap joint may have a greater endurance than a comparable 3/4 inch lap joint - both tested to the same load history. This effect was not observed in this program for joints with $\pm$45 degree surface plies and their particular failure modes.

8. The estimation of life for the bonded B/Ep-Ti joints, using constant amplitude data and a linear damage (e.g., Miner's Rule) summation, is extremely unconservative. Life predictions were greater than 15 times the actual endurance found from tests under a flight-by-flight load spectrum.

9. The average static strength of the 3/4 inch lap joints was 35 percent greater than that for the 1/2 inch joints for specimens designed with ±45 degree surface plies.

10. A joint proof load, or a load near the limit strength of the joint, that is conducted prior to simulated flight loading, may heavily damage the joint. It will tend to reduce endurance from that experienced with the same load(s) conducted after a break-in period for the bonded joint. That is, the numerous low 'working-in' loads of flight-by-flight loading tend to reduce the effect of a high load conducted later on. An initial proof test to 74% of the maximum load in the proof test spectrum of this program load caused a reduction in mean endurance to 90% of that experienced with no proof load. However, the effects of practical proof loading for joints tested to long endurance need to be determined.

11. The data scatter or coefficient of variation for the endurance of the composite joints was roughly three times greater for the high endurance joints (0 degree ply at the bond surface interface) that were loaded to fail at 1 to 2 lifetimes than for the joints with ±45 degree plies at the faying surfaces, which failed in the same endurance span but under lower cyclic stresses.

12. Temperatures achieved directly at the cut point in diamond wheel machining situations on bonded titanium joints did not exceed 360°F and were generally below 250°F in the cut zone. These temperatures, related to the type and quantity of cooling used, are considered to be representative of those occurring during the slicing of B/Ep-Ti specimens from slab-cured panels. Although these temperatures should not have

been chemically damaging to the constituents of the joints, the thermal gradients produced may increase damage at the specimen edges. From strength and endurance data, conclusive edge effects were not observed between 1/2 inch and 1 inch wide joints in this program. However, one mode of failure, found on the wider joints indicated that the stress profiles did vary across the specimen width.

13. Scanning electron microscopy was useful in determining the stress direction in the laminating resin at the failure planes on the shear-failed 0 degree boron ply. Evidence of cyclic damage growth was not observed for reversed-load fatigue. However, a high resolution study at the boron-to-resin interface might indicate reversed micro-damage and the growth of a damage zone.

14. Age effects on strength and endurance were not observed over the three years in which joints were stored in an air conditioned office environment without special protection.

15. The frequency of applying random loads did not significantly affect endurance, comparing tests conducted at 1/2 Hz and 8 Hz.

16. A comparable program to this study should be conducted for graphite and other composite material systems. Temperatures and environment should be added factors to study.

17. Efforts to realistically test bonded structures under simulated conditions of stress, environment, temperature, and time must be based upon a thorough understanding of load spectrum, proof test, and time compression effects.

REFERENCES

1. Manning, S.D. Lemon, G.H. Waddoups, M.E., and Achard, R.T., "Composite Wing for Transonic Improvement - Volume III - Structural Reliability Study" AFFDL-TR-71-24, Volume III, November 1972.

2. Halpin, J.C., Jerina, K.L., and Johnson, T.A., "Characterization of Composites for the Purpose of Reliability Evaluation," Analysis of Test Methods for High Modulus Fiber and Composites, ASTM STP 521, American Society for Testing and Materials, 1973.

3. Hart-Smith, L.J., "Adhesive-Bonded Double Lap Joints," NASA CR-112235, January 1973.

4. Fehrle, A.C., Carroll, J.R., Freeman, S.M. et al, "Development of an Understanding of the Fatigue Phenomena of Bonded and Bolted Joints in Advanced Filamentary Composite Joints", AFFDL-TR-72-64, June 1972.

5. West, B.S., "Bonded Joints in Composite Structures," AFFDL-TR-73-99, November 1973.

6. Birchfield, E.B., Cole, R.T., and Impellizzeri, L.F. "Reliability of Step-Lap Bonded Joints," AFFDL-TR-75-26, April 1975.

TABLE 1

LOAD SUMMARY

Bending Moment (Y)	Incremental Bending Moment (ΔY)	Load Level	Loads per Mission	Test Load Amplitude (P) (lb)	Block Frequency (Hz) (Select - Random Spectrum)
-4.9	-7	T	.02	-980	1
-2.9	-5	R	.18	-580	1
-0.9	-3	S	1.0	-180	1/4
-0.9	-3	Q*	3.7	-180	2
1.1	-1	P*	23.1	220	10
2.1	0	1g	-	420	-
3.1	1	M	182.1	620	Omitted All Tests
5.1	3	A	66.	1020	10
7.1	5	B	23.1	1420	10
9.1	7	C	9.9	1820	5
11.1	9	D	3.7	2220	2
13.1	11	E	1.35	2620	1
15.1	13	F	.57	3020	1/2
17.1	15	G	.25	3420	1/2
19.1	17	H	.08	3820	1/4
21.1	19	I	.02	4220	1/4
-	-	Proof Load	-	4060	-

NOTES:
a. Each load (A-I) was followed by a return to the 1g load
b. *Indicates loads that were included as the valleys for loads D and B, respectively.
c. Load S of magnitude Q and frequency 1/4 Hz concluded each mission as a ground load.
d. Loads greater than +1g above the 1g cruise numbered 104.97 per mission.
e. Loads less than 1g cruise numbered 28 per mission.
f. Total loads used in the Random Spectrum numbered 133 per mission (flight loads) plus one S level load to end each mission.
g. Symbols are defined in Section IV, units for Y and ΔY are 10^6 in lb.

TABLE 2

STATIC TEST STATISTICS

TEST DATE	SCHEDULE	LAP LENGTH (in)	WIDTH (in)	MEAN LOAD (lb)	COEF. VAR (%)	NUMBER OF SPECIMENS	NOTES
Oct 72	40	1/2	1	6583	4	6	Mean = 6675 lb
Oct 72	50	1/2	1	6767	4	6	P^{B}_{UT} = 6089 lb
Sep 73	50	1/2	1	6700	3	4 } Paired	
Sep 73	50	3/4	1	9040	5	4 } Joints	Incl. 1 Boron failure
Sep 73	50	3/4	1	9200	3	4	{ No 1/2" lap test Incl. 2 Boron failures
Mar 74	50	1/2	1/2	3271	0.5	4	
Mar 74	50	3/4	1/2	4593	2	4	
Nov 74	40	1/2	1	6480	1	3	
Apr 75	40	1/2	1/2	2782*	3	3	
Feb 76	50	1/2	1/2	3283	10	4 } Paired	
Feb 76	50	3/4	1/2	4493	4	4 } Joints	

Notes:

a. P^{B}_{ut} = 'B' Allowable, i.e., probability of strength exceeding the allowable is 90% with 95% confidence.

b. Average strength of all 1-inch-wide SCHEDULE 40 tests is 6548 lb, and of SCHEDULE 50 tests is 6740 lb.

c. *These tests were inadvertently conducted with a non-axial load and, therefore, indicated a reduced strength.

d. All specimens were fabricated in February 1972.

TABLE 3

STATIC TEST DATA

DATE	SPECIMEN NO.	WIDTH (in)	FAILURE LOAD 1/2" Lap (lb)	FAILURE LOAD 3/4" Lap (lb)
OCT 72	42-2	1	6680	-
	42-6	1	6662	-
	42-11	1	6426	-
	44-2	1	6926	-
	44-5	1	6184	-
	44-9	1	6619	-
	51-2	1	6433	-
	51-5	1	6857	-
	51-9	1	6583	-
	53-2	1	6930	-
	53-5	1	7163	-
	53-11	1	6636	-
SEP 73	53-71	1	6720	8700
	51-8	1	6440	8620
	53-22	1	6920	9340
	52-5	1	6720	9500B*
	52-29	1	-	8990B
	53-62	1	-	9450
	52-4	1	-	8980B
	53-26	1	-	9380
MAR 74	52-1	1/2	3275	4650
	52-7	1/2	3240	4675
	53-1	1/2	3360	4620
	53-7	1/2	3210	4425
NOV 74	42-48	1	6390	-
	42-22	1	6550	-
	43-22	1	6500	-

TABLE 3 (Cont'd)
STATIC TEST DATA

DATE	SPECIMEN NO.	WIDTH (in)	FAILURE LOAD 1/2" Lap (lb)	FAILURE LOAD 3/4" Lap (lb)
APR 75	42-7	1/2	2680	-
	43-7	1/2	2840	3795B
	42-32	1/2	2825	3955B
FEB 76	53-33	1/2	2810	4250
	53-41	1/2	3280	4500
	53-47	1/2	3460	4500
	53-52	1/2	3580	4720

*B signifies failure in boron adherend

TABLE 4

ENDURANCE - SCHEDULE 50 TESTS

SPECIMEN NO.	SPECTRUM	EQUIV. LIFETIMES 1/2 INCH LAP	LOAD AT FAILURE	RESIDUAL STRENGTH 3/4 INCH LAP (lb)
52-3	BASELINE	1.048	I	8380
52-8		1.198 $\bar{X}$=1.07	I	3560C $\bar{X}$=8853
52-23		0.974 γ=9%	I	9080 γ=5%
52-28		1.048	I	9100
53-3	BASELINE	1.161	H	9150
53-8		1.461	I	9080
53-23		1.499	I	9290 $\bar{X}$=8525
53-28		1.426 $\bar{X}$=1.26	I	9000 γ=17%
53-43		1.349 γ=26%	I	8475 $\bar{X}_7$=9034
53-48		1.199	I	9075B γ_7=3%
53-63		1.499	I	4960S
53-68		0.524	I	9170
53-9	TRUNCATE:	2.007	I	8975 $\bar{X}$=8258
53-49	A,B	2.398 $\bar{X}$=2.59	I	9060 γ=15%
52-10		2.960 γ=18%	I	6385S $\bar{X}_3$=8882
52-26		3.000	I	8610 γ_3=3%
52-30	TRUNCATE:	2.323	I	9300
52-24	A	2.800 $\bar{X}$=2.52	H	9075 $\bar{X}$=8944
51-7		2.735 γ=12%	I	8500 γ=4%
53-65		2.211	I	8900
52-31	TRUNCATE:	4.309	I	8900
53-6	F,G,H	4.722 $\bar{X}$=7.43	I	8780 $\bar{X}$=8774
53-25		8.582 γ=37%	I	7960 γ=5%
52-2		10.528	I	9180
52-11		9.100	I	9050

TABLE 4 (Cont'd)

ENDURANCE - SCHEDULE 50 TESTS

SPECIMEN NO.	SPECTRUM	EQUIV LIFETIMES 1/2 INCH LAP	LOAD AT FAILURE	RESIDUAL STRENGTH 3/4 INCH LAP (lb)
53-4	TRUNCATE:	7.458	I	8950
52-6	G,H	8.207 $\bar{X}$=6.802	I	9160 $\bar{X}$=8933
53-70		6.671 γ=21%	I	8900 γ=2%
51-3		4.872	I	8720
53-50	RANDOM:	0.433	I	-
53-24	1/2 Hz	0.563 $\bar{X}$=.4595	I	-
53-44		0.372 γ=17%	I	-
53-29		0.470	I	-
53-30	RANDOM:	0.490	F	-
53-69	8 Hz	0.403 $\bar{X}$=.4823	I	-
53-64		0.443 γ=17%	F	-
53-46		0.593	H	-

TABLE 4 (Cont'd)

ENDURANCE - SCHEDULE 50 TESTS

SPECIMEN NO.	SPECTRUM	CYCLES TO FAILURE	P_{max} (lb)	P_{min} (lb)	RESIDUAL STRENGTH 3/4 INCH LAP (lb)
51-6	CONST. AMPLITUDE:	736C*	4060	-812	8750
53-31	R= - 0.2	7,541 $\bar{X}$=7713	4060	-812	9210 $\bar{X}$=8796
53-10	5 Hz	7,680 γ=3%	4060	-812	8830 γ=4%
52-9		7,920	4060	-812	8395
51-4	CONST. AMPLITUDE	274,124	2620	-524	8180
52-22	R= - 0.2	227,392 $\bar{X}$=333,462	2620	-524	9020B $\bar{X}$=8695
52-27	5 Hz	486,012 γ=34%	2620	-524	8680 γ=4%
53-66		346,319	2620	-524	8900
53-32**	CONST. AMPLITUDE:	6,550 $\bar{X}$=6797	2110	210	-
53-27**	P_{min}=420 lb/in	7,030 γ=4%	2110	210	-
53-21**	5Hz	6,810	2110	210	-
53-51		2,455C***	5000	420	-
53-42		850 $\bar{X}$=895	5000	420	-
53-45		940	5000	420	-
53-67**		878,000 Runout	1510	210	-
53-12**		186,505 $\bar{X}$=556,795	1510	210	-
52-12**		927,085	1510	210	-

NOTES: a) B=failure in boron outside joint; C=censored data, S=suspect data; subscript 3 or 7 indicate statistical properties for highest 3 or 7 data points, respectively; $\bar{X}$=mean of data; γ = coefficient of variation for data.

b) **Specimens with this designation were 1/2 in. width, all other specimens were 1 in. wide.

c) Runout - Specimen removed from fatigue test before failure.

d) *Abnormal proof test strain; ***Problems encountered bringing test equipment into load, censored data point.

TABLE 5

SPECTRUM TESTS - SCHEDULE 50

SPECTRUM	MEAN LIFETIMES	RANGE LIFETIMES	NUMBER OF SPECIMENS	COEF. VAR. (%)	MEAN RESIDUAL STRENGTH 3/4" Lap (lb)
Baseline (Batch 53)	1.26	1.0	8	26	9034
Baseline (Batch 52)	1.07	0.2	4	9	8853
Average Baseline	1.20	1.0	12	24	8980
Truncate Loads:					
A	2.52	0.6	4	12	8944
A&B	2.59	1.0	4	18	8882
G&H	6.80	3.3	4	21	8933
F,G,&H	7.45	6.2	4	37	8774
Random (1/2 Hz)	.456	0.2	4	17%	--
Random (8 Hz)	.476	0.2	4	17%	--

NOTES:

a. All specimens 1 in. wide with $\pm 45^{\circ}$ plys on faying surfaces

b. Mean Residual strengths are with suspect values removed, see Table 4

TABLE 6

ENDURANCE - SCHEDULE 40 TESTS

SPECIMEN NO.	WIDTH (in)	KP_I (lb)	EQUIVALENT LIFETIMES	LOAD AT FAILURE	PROOF LOAD (lb)
43-3	1	4220	7.44	Failure in 3/4 inch lap	4060
42-29	1	5000	4.21	H	4060
44-7	1	5500	Test Abort	-	4060
44-4	1	5500	.59	H	4060
43-10	1	5500	.93	G	4060
43-25	1	5400	2.49	H	4060
43-24	1	5400	2.69	H	4060
43-28	1	5450	2.33	E	4060
44-6	1	5450	.55	G	4060
42-25	1	5450	.85	H	4060
43-11	1	5450	1.35	I	4060
44-8	1	5500	.39	Failure in 3/4 inch lap	No Proof
42-27	1/2	2725	1.35	I	No Proof
43-27	1/2	2725	1.20	I	No Proof
43-32	1/2	2725	2.11	-	No Proof
43-12	1/2	2750	1.21	I	No Proof
43-21	1/2	2750	.98	F	No Proof
42-12	1/2	2750	1.00	G	No Proof
42-1	1/2	2750	.45	H	2030
42-21	1/2	2750	.60	H	2030
43-1	1/2	2750	.90	I	2030
43-31	1	5450	1.99	I	No Proof
42-46	1	5450	1.27	H	No Proof
42-23	1	5450	2.70	I	No Proof
42-45	1	5450	.09	H	6000
42-31	1	5450	1.12	H	6000
42-10	1	5450	.43	-	6000
43-30	1	5450	1.76		6000
42-44	1	5450	.82	H	6000
42-28	1	5450	1.95	H	5500
43-29	1	5450	4.26	H	5500
42-49	1	5450	.37	I	5500
42-47	1	5450	.89	-	5500

TABLE 7

ENDURANCE STATISTICS - SCHEDULE 40

Width (in.)	Maximum Load KP_I (lb)	Factor K	Maximum Load $\%P^M_{UT}$	Maximum Load $\%P^M_{LT}$	Proof Load (lb)	Number of Specimens	Mean Lifetimes	Coef. Var. (%)
1	4220	1	65	97	4060	1	7.4	—
1	5000	1.18	76	114	4060	1	4.2	—
1	5400	1.28	82.5	124	4060	2	2.6	—
1	5450	1.29	83.3	125	0	3	2.0	36
1	5450	1.29	83.3	125	4060	4	1.3	61
1	5450	1.29	83.3	125	5500	4	1.9	92
1	5450	1.29	83.3	125	6000	5	0.8	76
1	5500	1.32	84.0	126	4060	2	0.8	—
1/2	2750	1.32	84.0	126	0	3	1.1	12
1/2	2750	1.32	84.0	126	2030	3	.7	36
1/2	2725	1.29	83.3	125	0	3	1.6	95

NOTES:
a. Tests were with Baseline Spectrum adjusted by multiplying all loads by a factor K.
b. 1 in. wide mean strength, P^M_{UT}=6548 lb = Mean of all tests run in Oct 72 and Nov 74.
c. 1/2 in. wide mean strength assumed at 6548 ÷ 2 = 3274 lb as compared to the static strength of 2782 lb noted in actual tests, where the load was inadvertently non-uniform.
d. Mean limit strength = P^M_{LT}=2/3 P^M_{UT} for this comparison.

TABLE 8

PROOF TEST/ENDURANCE ANALYSIS - SCHEDULE 40

Width	Number of Specimens	Proof Load			Mean Lifetimes	
		(lb)	$\%P^{M}_{UT}$	$\%P_I$	All Data	Deleted*
1	3	none	0	0	1.99	-
1	4	4060	62	75	1.27	-
1	4	5505	84	101	1.87	1.07
1	5	6000	92	110	0.84	-
1/2	3	none	0	0	1.55	-
Pooled 1 & 1/2	6 (from above)	none	0	0	1.77	

NOTES: All specimens 1 inch wide with tolerances of $\pm$0.7%

P_I for all 1 inch tests = 5450 lb, P_I 2725 lb for the 1/2 inch test

P^{M}_{UT} = Mean strength of SCHEDULE 40 specimens = 6548 lb

P_I = 5450 lb

*One data point (4.26 lifetimes) was deleted to show the effect on mean endurance of this extremely long-life specimen. This specimen endurance exceeded all other endurances (30 data points) for P_I 5000 lb; see Table 6.

TABLE 9

CUMULATIVE DAMAGE

Load Level	Cycles Per Lifetime (CPL)	N_i (Cycles)	CPL/N_i	(CPL/N_i) X (Lifetimes), from Spectrum Tests				
				Lifetime:	1.26	2.52	2.59	6.80	7.45
				Spectrum:	Baseline	-A	-A-B	-G-H	-F-G-H
I	26.68	5,100	.0052		.0066	.013	.013	.036	.040
H	106.72	14,000	.0076		.0096	.019	.020	-	-
G	333.50	40,000	.0083		.0105	.021	.021	-	-
F	760.38	114,000	.0067		.0084	.017	.017	.045	-
E	1,800.90	333,462	.0054		.0068	.014	.014	.037	.040
D	4,935.80	$0.94 \cdot 10^6$	.0053		.0066	.013	.014	.036	.039
C	13,206.60	$2.6 \cdot 10^6$	.0051		.0064	.013	.013	.035	.038
B	30,815.40	$7.4 \cdot 10^6$	.0042		.0053	.011	-	.028	.031
A	88,044.00	$21 \cdot 10^6$	.0042		.0053	-	-	.028	.031
				$\Sigma(n_i/N_i)$:	.0655	.121	.112	.245	.219

Notes:

(a) Cycles per Lifetime based on data from Table 1 and 1334 missions per Lifetime.
(b) N_i=number of constant amplitude cycles at the specific load level, from (S-N) curve at $R=\frac{\text{min load}}{\text{max load}}=-0.2$, see Figure 12.
(c) n_i=total number of load occurrences at the indicated load level at time of failure.
(d) Spectrum Test Data from Table 5, spectrums shown above are the baseline deleting the levels shown (e.g., minus A and B).
(e) $\Sigma(n_i/N_i)$ for Random Load tests are 0.0237 and 0.248 for the 1/2 Hz and 8 Hz cyclic rates, respectively.

TABLE 10

PREDOMINANT FAILURE MODE CHARACTERISTICS

Test Type	Predominant Side for First Failure	Area for Each Failure Type (%)		Failure Pattern and Frequency
		Scrim Side	Non Scrim Side	
Static Sch. 40	90% S	10-70B Rem. C+A_B	40-70C Rem. A_B+B	40-1T (60%) 40-2 (40%)
Static	95% NS	60-80B	60-90A_B	50-2 (70%)
Sch. 50	100% NS	30-80B Rem. C+D	90-95B Rem. C+D	50-1 (30%)
Fatigue	100% S	50-80B	10-90B	40-2 (65%)
Sch. 40	60% S	80-99B Rem. C	60-90B Rem. C	40-1T (35%)
Reversed Load Fatigue Sch. 50	98%S	80-90B Rem. D	40-70B Rem. D	50-1 (100%)
Tension-Tension Fatigue Sch. 50	65% NS	40-60B Rem. D.	70-80B Rem. D	50-1 (100%)

Notes:
(a) *=Baseline and constant amplitude fatigue with tensile/compressive stresses.
(b) Adhesive failure at the titanium surface (A_T) was seldom encountered and where observed it was limited to about 20% of the area.
(c) Failure Patterns and the definitions for the failure type code are shown in Figure 13.
(d) Rem. indicates remainder of the failure area. Var. indicates a scattered failure pattern.
(e) S indicates scrim side, NS indicates side without a balance scrim.

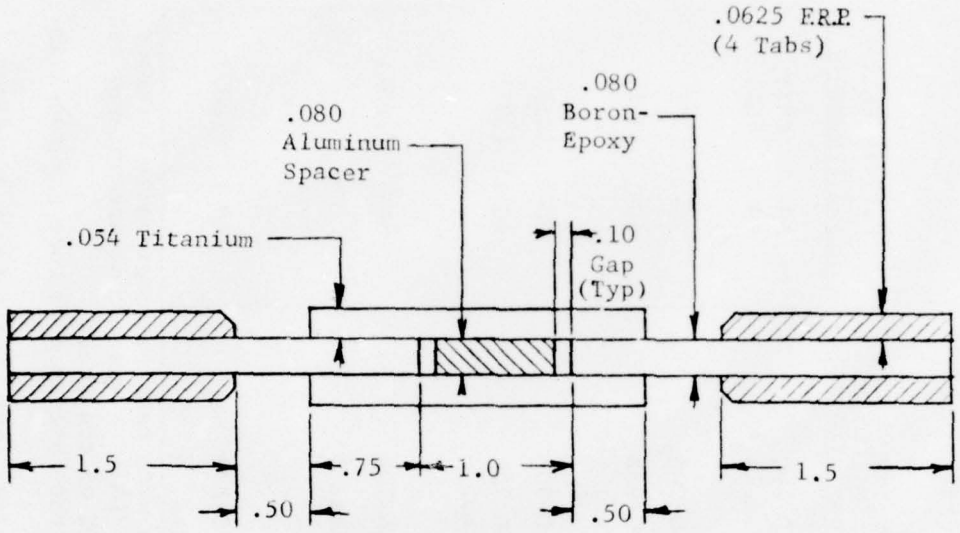

NOTES:

1. 0° Direction ⟶
2. Specimen Width - 1.0 and 0.5 inch
3. All components bonded in a single operation
4. Material:

Titanium	6Al-4V annealed	
Boron/Epoxy	Schedule 40 $[0/\pm45/0]_{2S}$	Narmco 5505, 4 mil fiber Precured
	Schedule 50 $[\pm45/0_2]_{2S}$	
Tabs	Glass Epoxy, 45° bevel	
Adhesive	Hysol 951, nominal cured thickness = .005 inch	
Spacer	Aluminum, .080 inch thickness, bonded to titanium	

Figure 1. Specimen Design

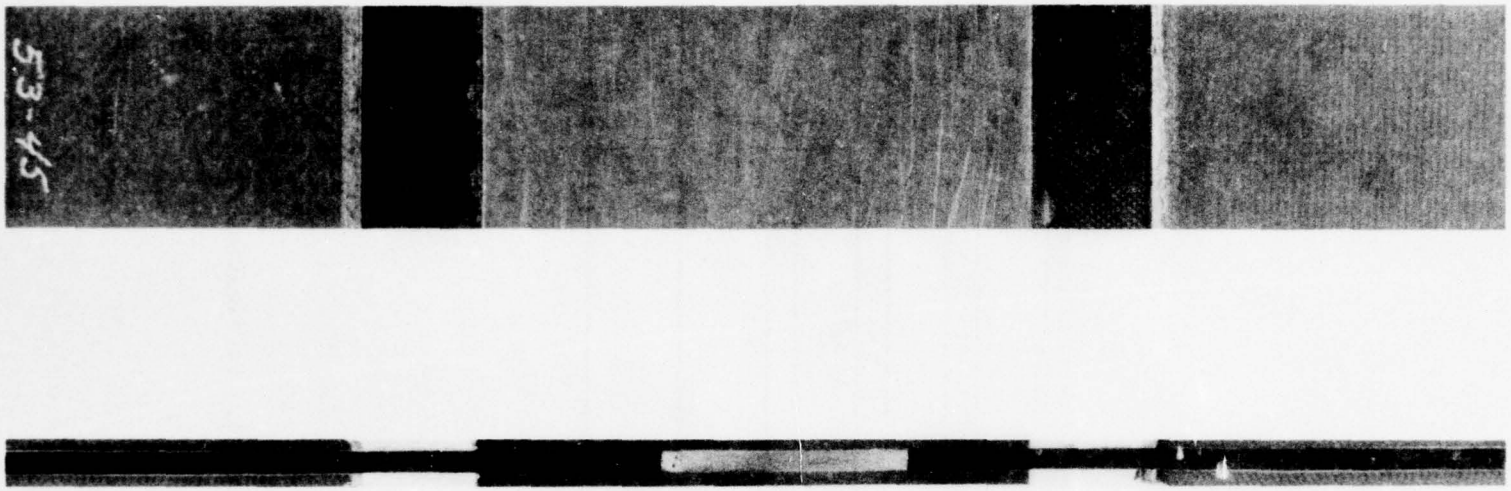

Figure 2. Finished Specimen

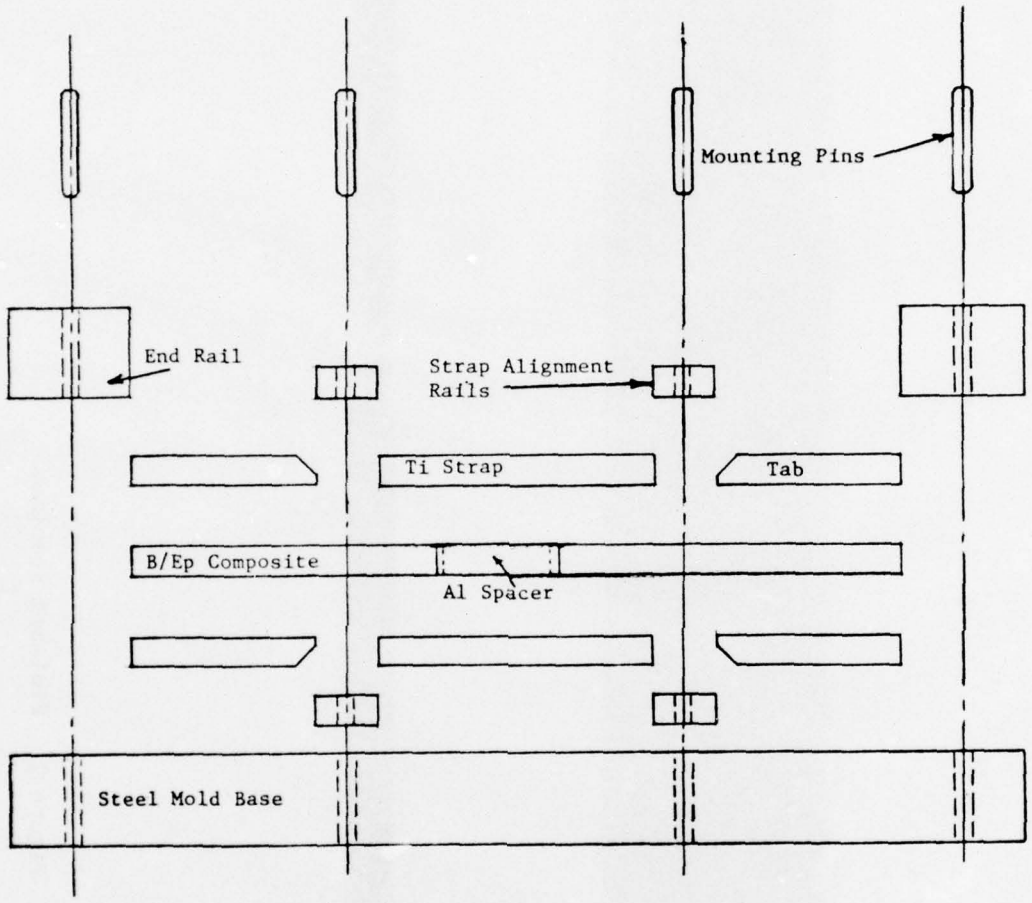

Figure 3. Fabrication Fixture

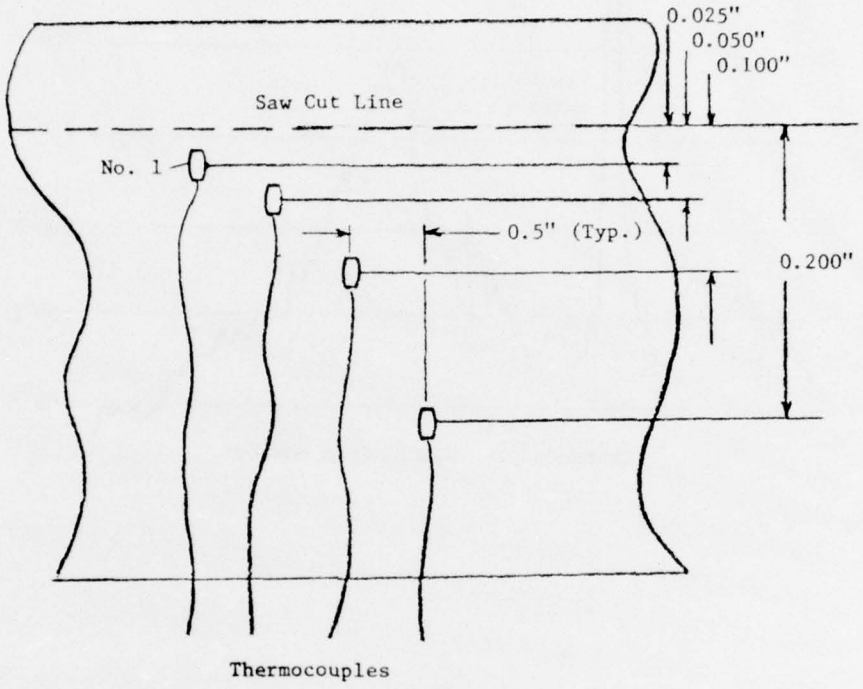

Figure 4. Bonded Coupon for Cutting Temperature Experiment

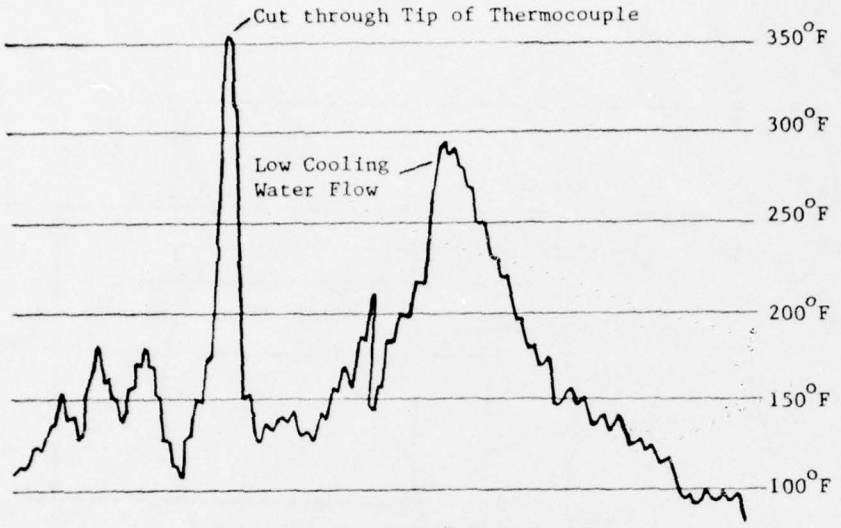

Figure 5. Saw-Cut Bondline Temperatures

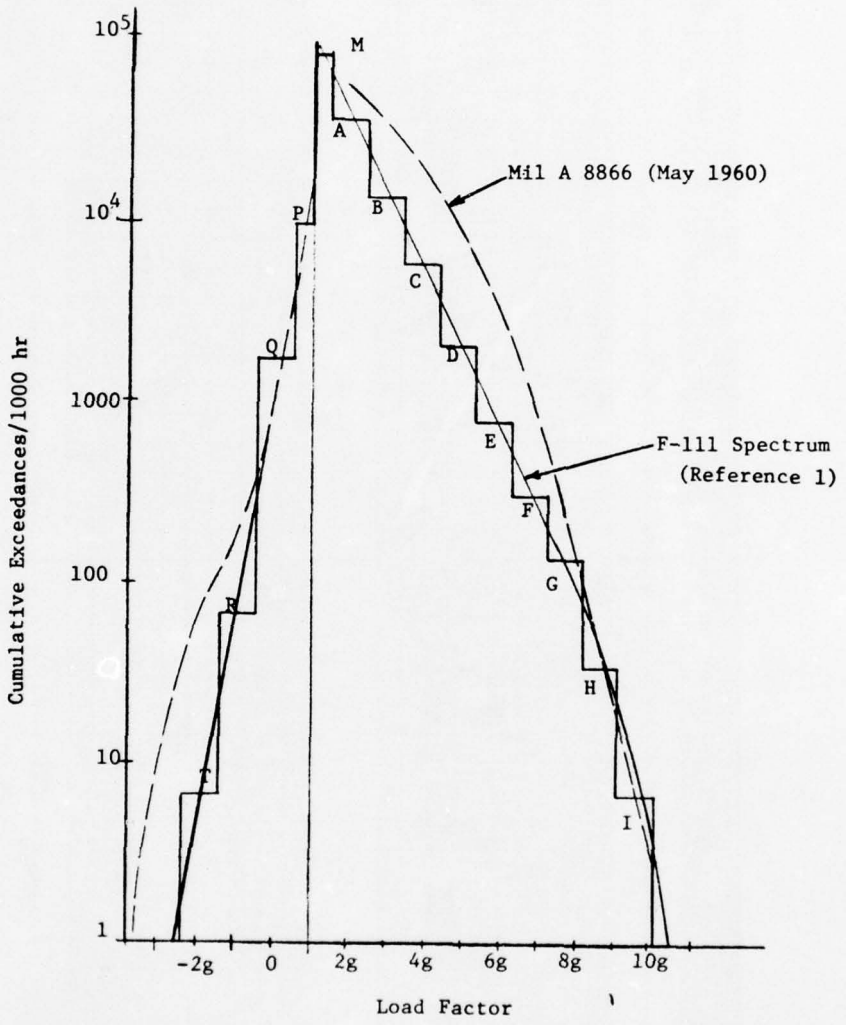

Figure 6. Maneuver Loads

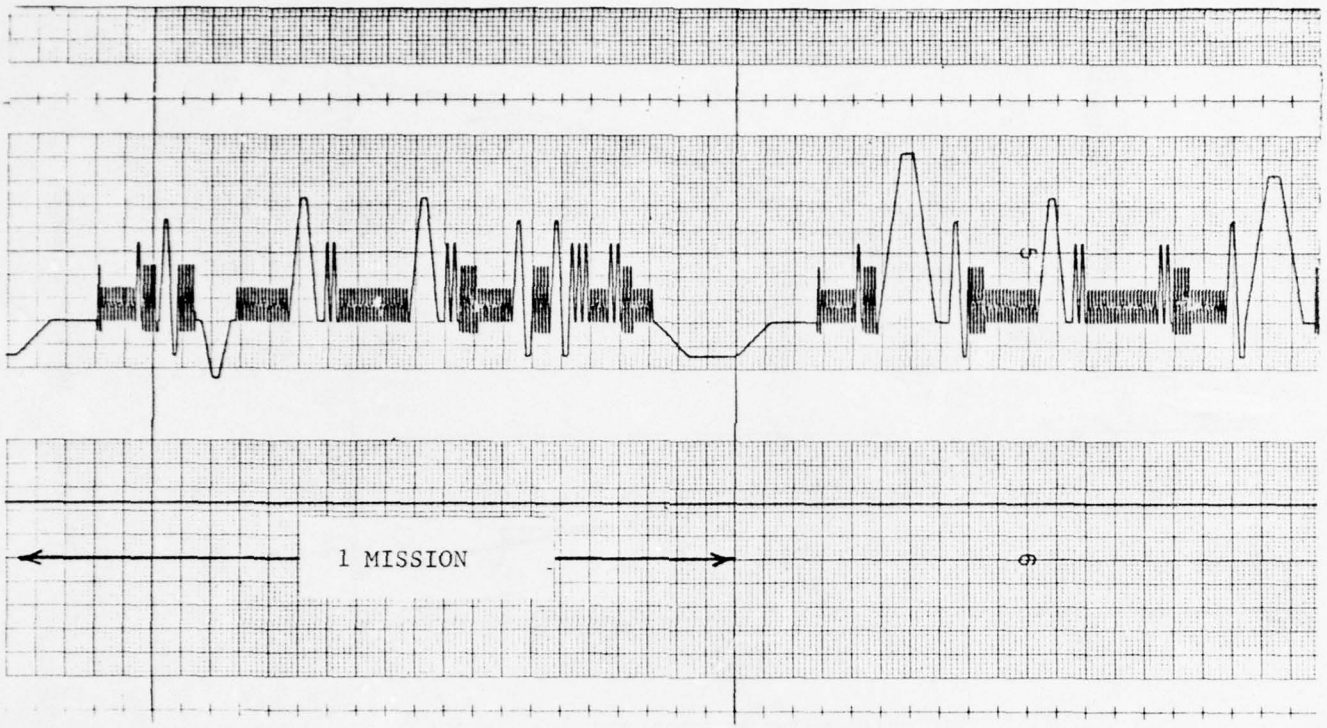

Figure 7. Select-Random Load Spectrum

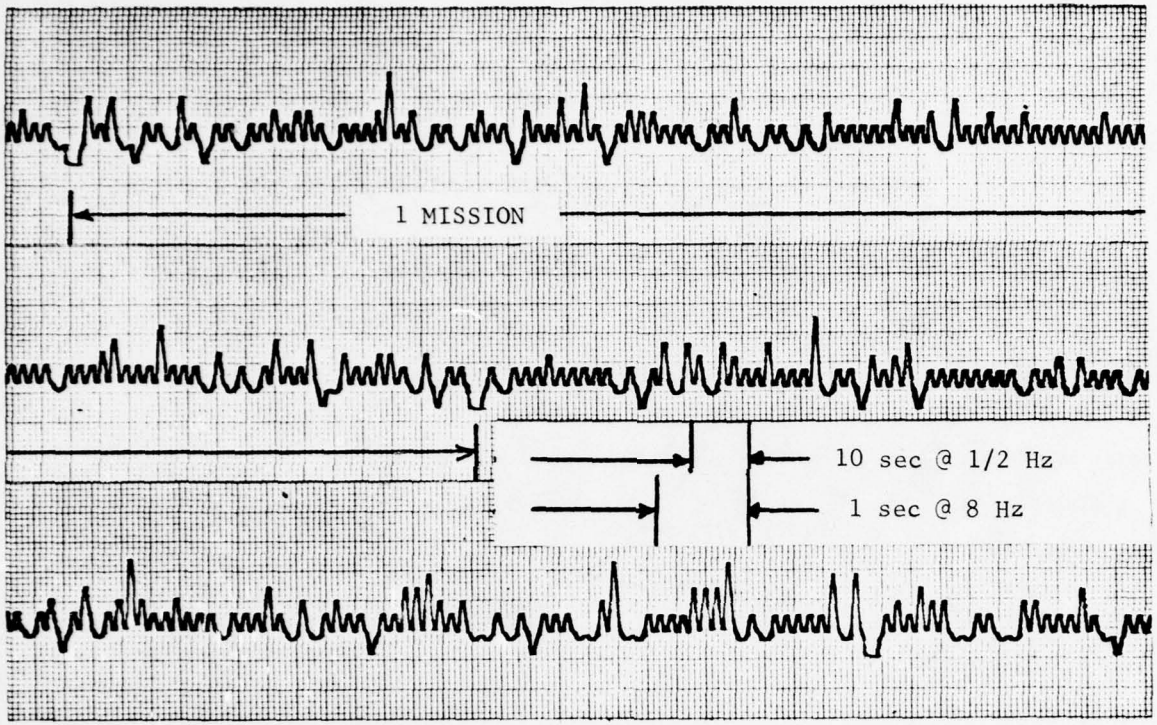

Figure 8. Random Generation Load Spectrum

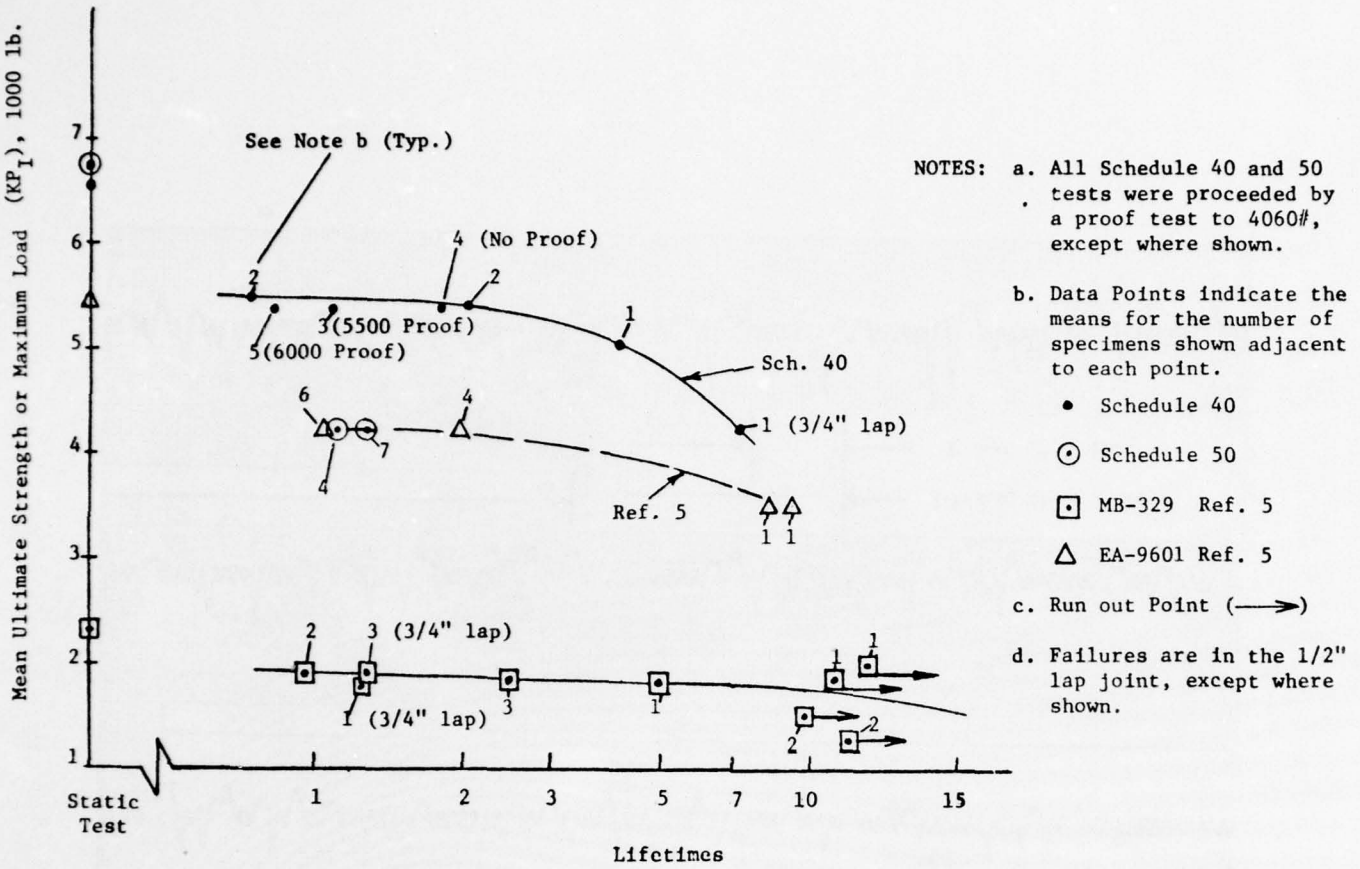

NOTES:

a. All Schedule 40 and 50 tests were proceeded by a proof test to 4060#, except where shown.

b. Data Points indicate the means for the number of specimens shown adjacent to each point.

- • Schedule 40
- ⊙ Schedule 50
- ⊡ MB-329 Ref. 5
- △ EA-9601 Ref. 5

c. Run out Point (⟶)

d. Failures are in the 1/2" lap joint, except where shown.

Figure 9. Endurance - Baseline Load Spectrum

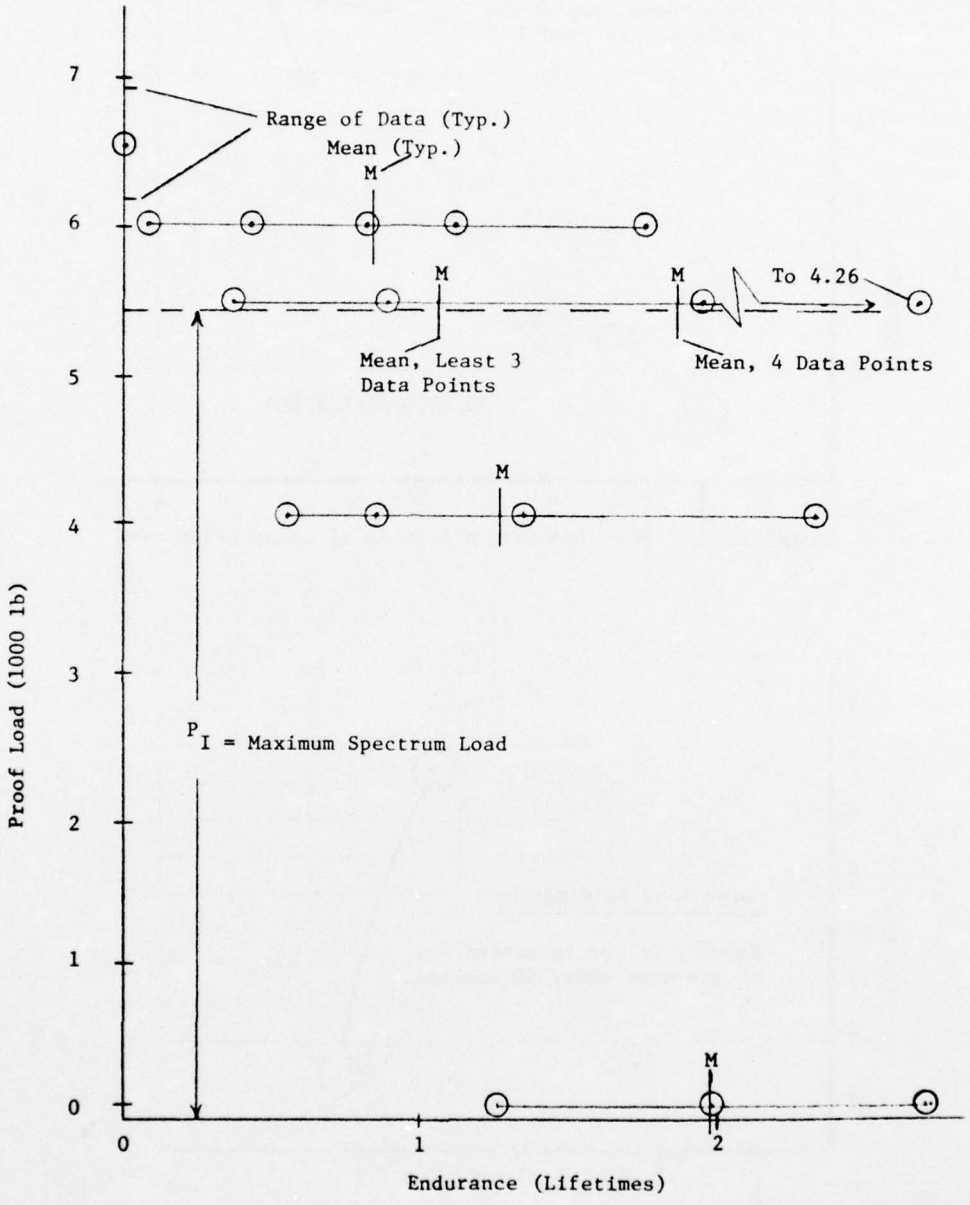

Figure 10. Effect of Proof Load-Schedule 40

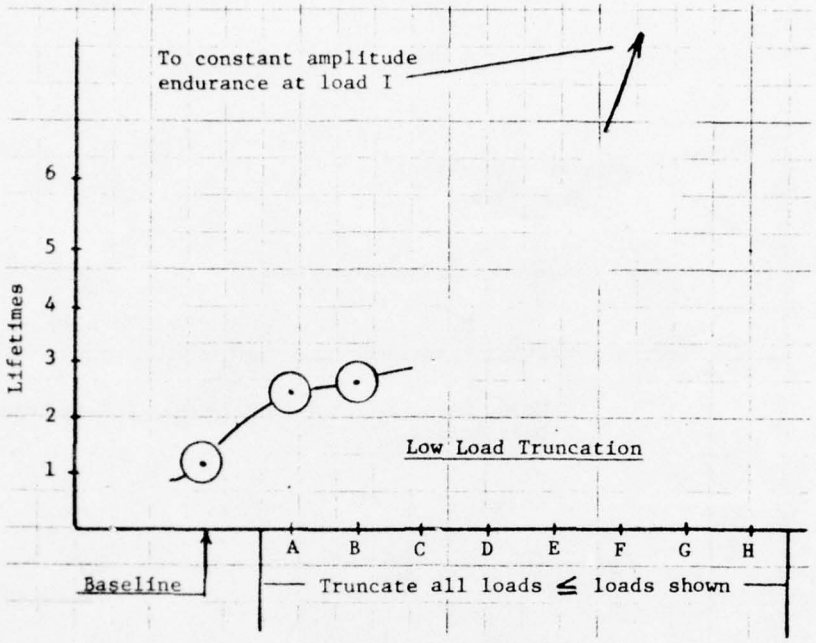

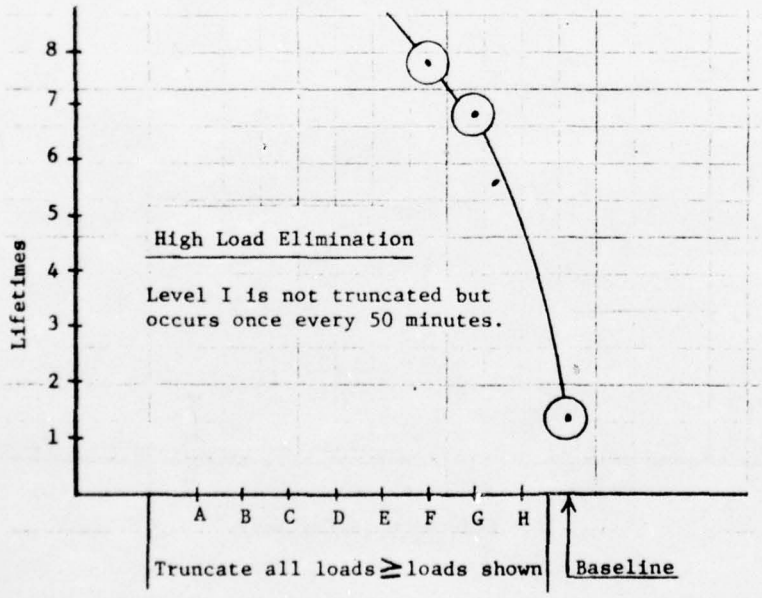

Figure 11. Load Truncation-Schedule 50

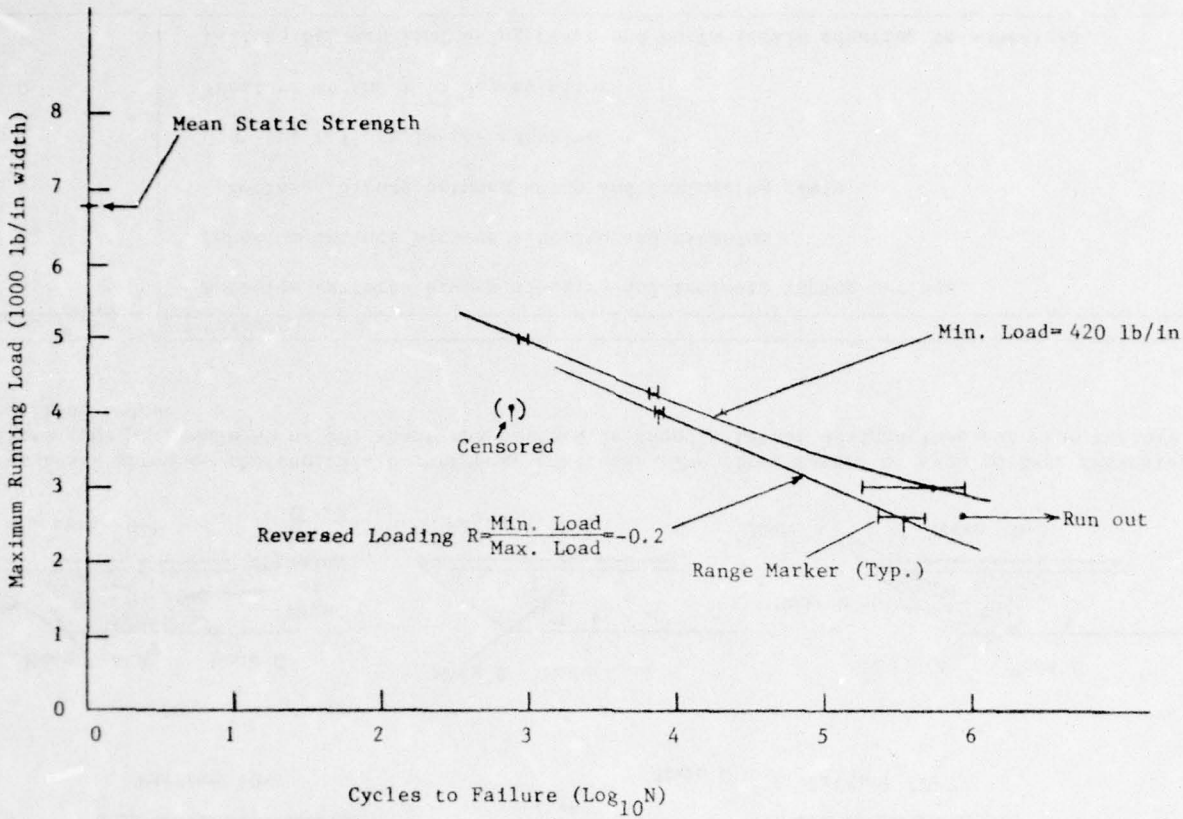

Figure 12. Constant Amplitude Tests-Schedule 50

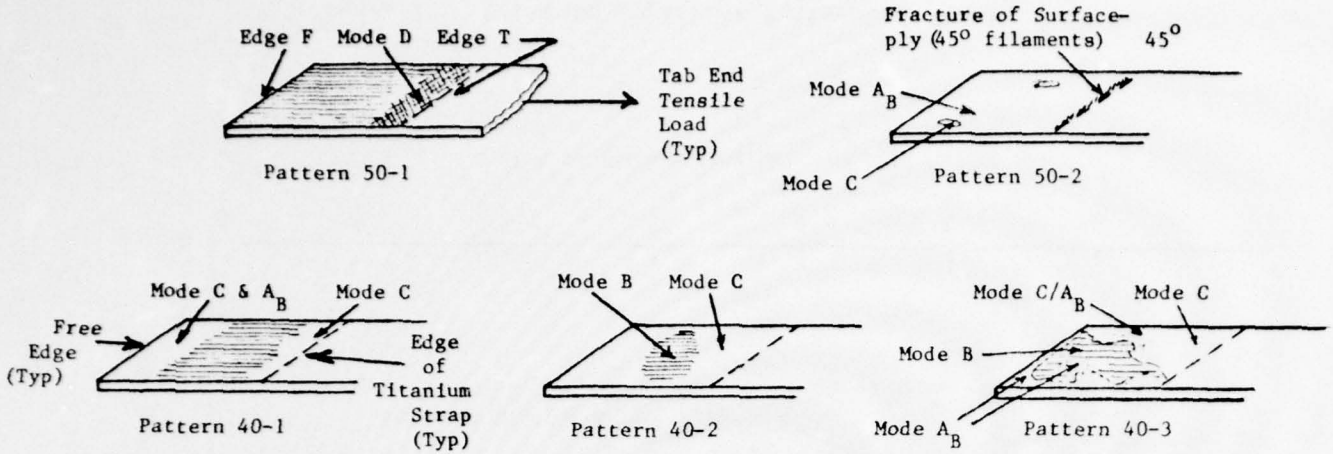

Patterns are shown on the central, boron/epoxy adherend. The first number of each pattern indicates the specimen type (Schedule 40 or 50) where the pattern is found. Letter designations over the failure areas are defined below.

Failure Types	Features
A_B	Adhesive failure between adhesive and laminate faying surface
A_T	Adhesive failure between adhesive and titanium
B	Interface failure between boron and laminating resin
C	Cohesive failure in the adhesive
D	Fracture in the $\pm$ 45 degree plies
S	Failure between laminating resin and scrim (resin adhering to adhesive)

Figure 13. Failure and Modes Patterns

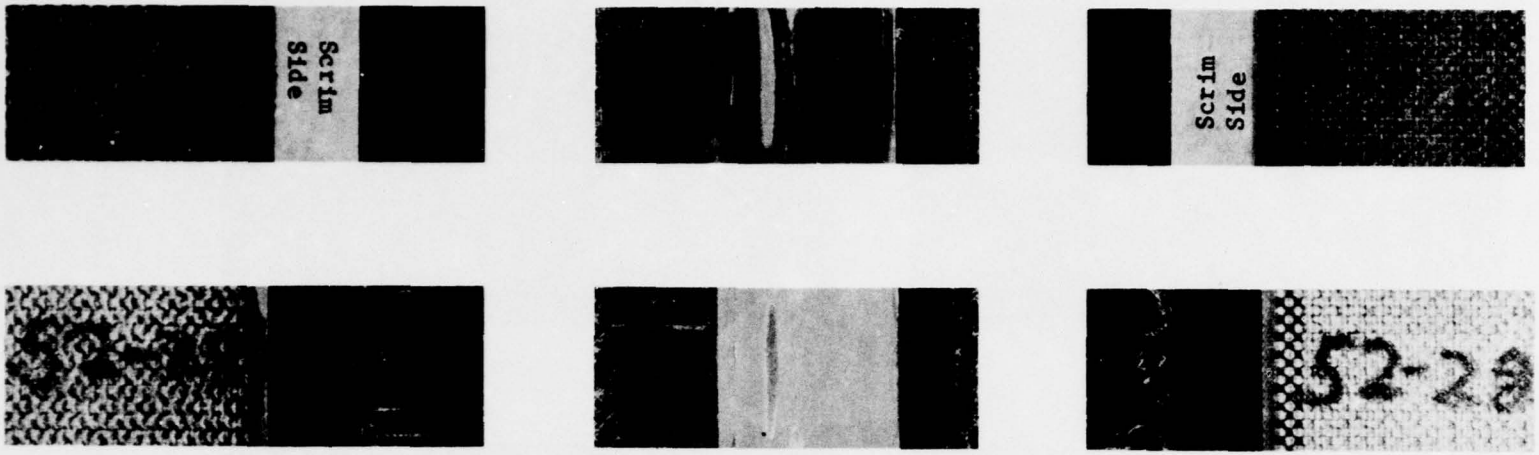

Figure 14. Typical Specimen Failure - Fatigue - Schedule 50.

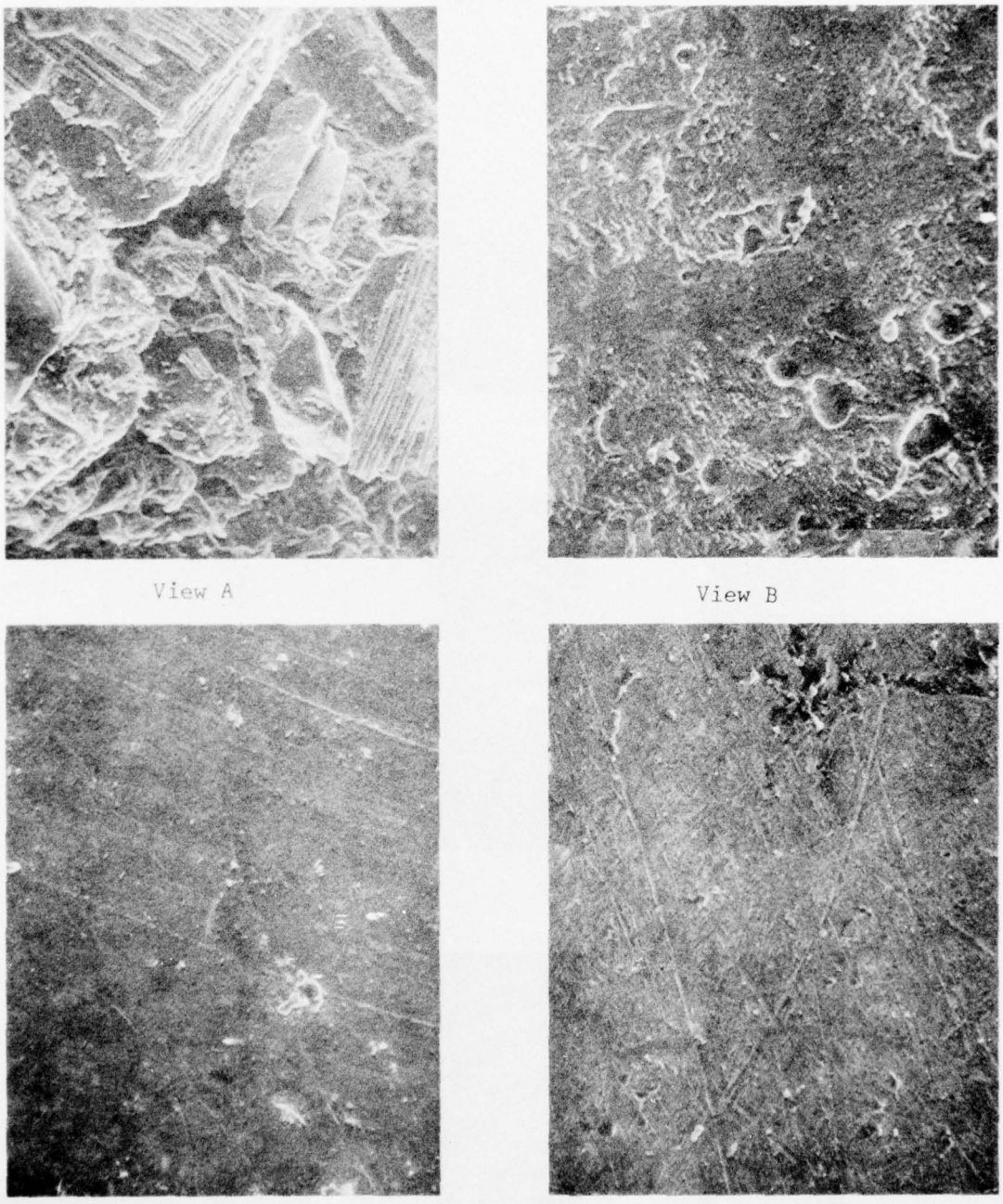

View A

View B

View C

View D

Figure 15. Typical Failed Areas on Titanium Strap, 150X.

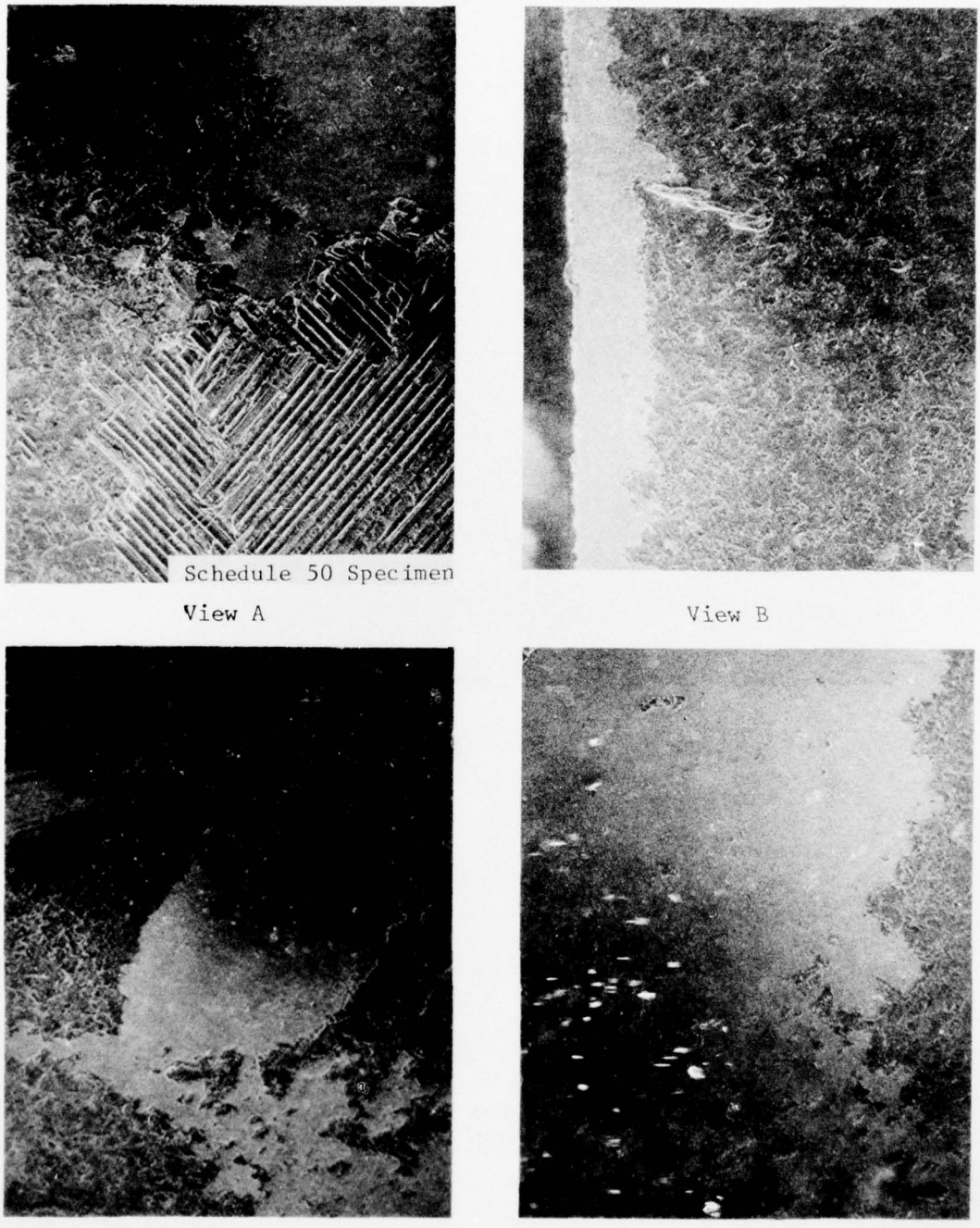

Figure 16. Typical Failed Areas on Titanium Strap, 15X.

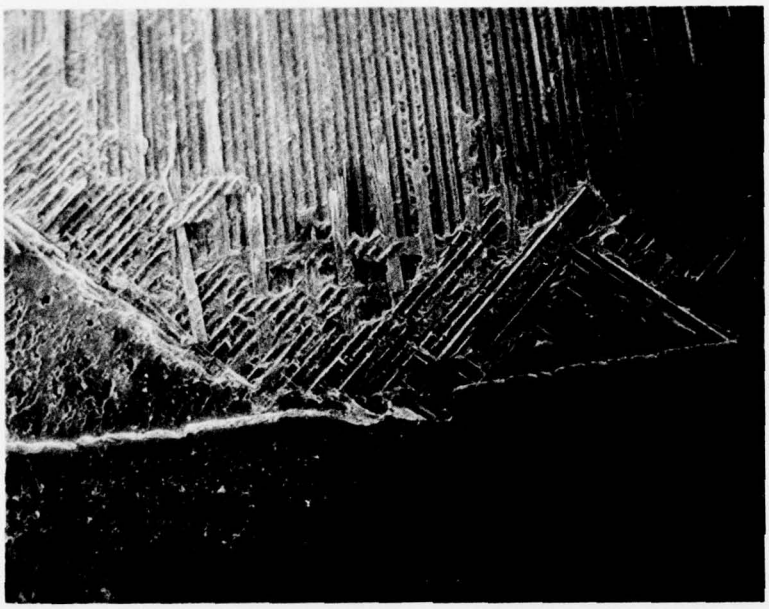

15X

Figure 17. Typical Failed Appearance of Boron/Epoxy under Titanium Strap Edge.

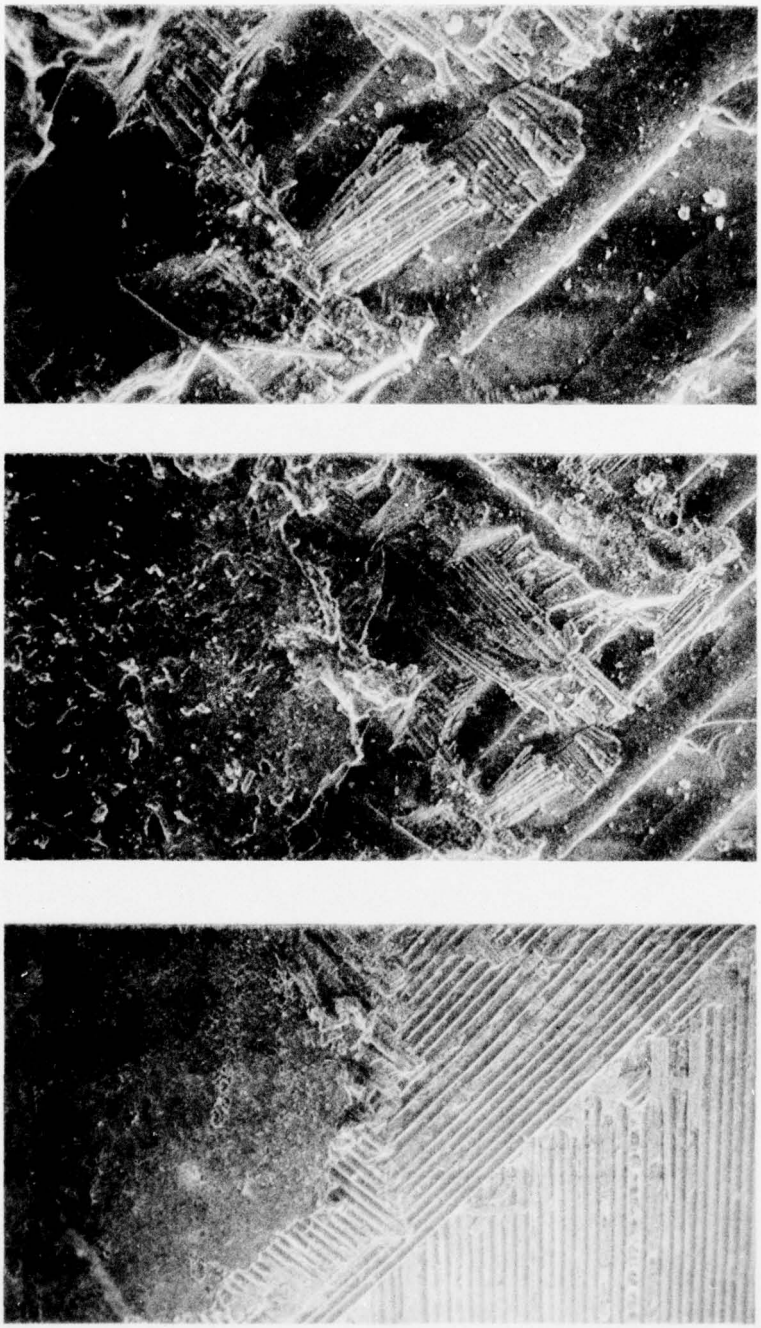

Figure 18. Three magnifications of Failed Boron/Epoxy Surface.

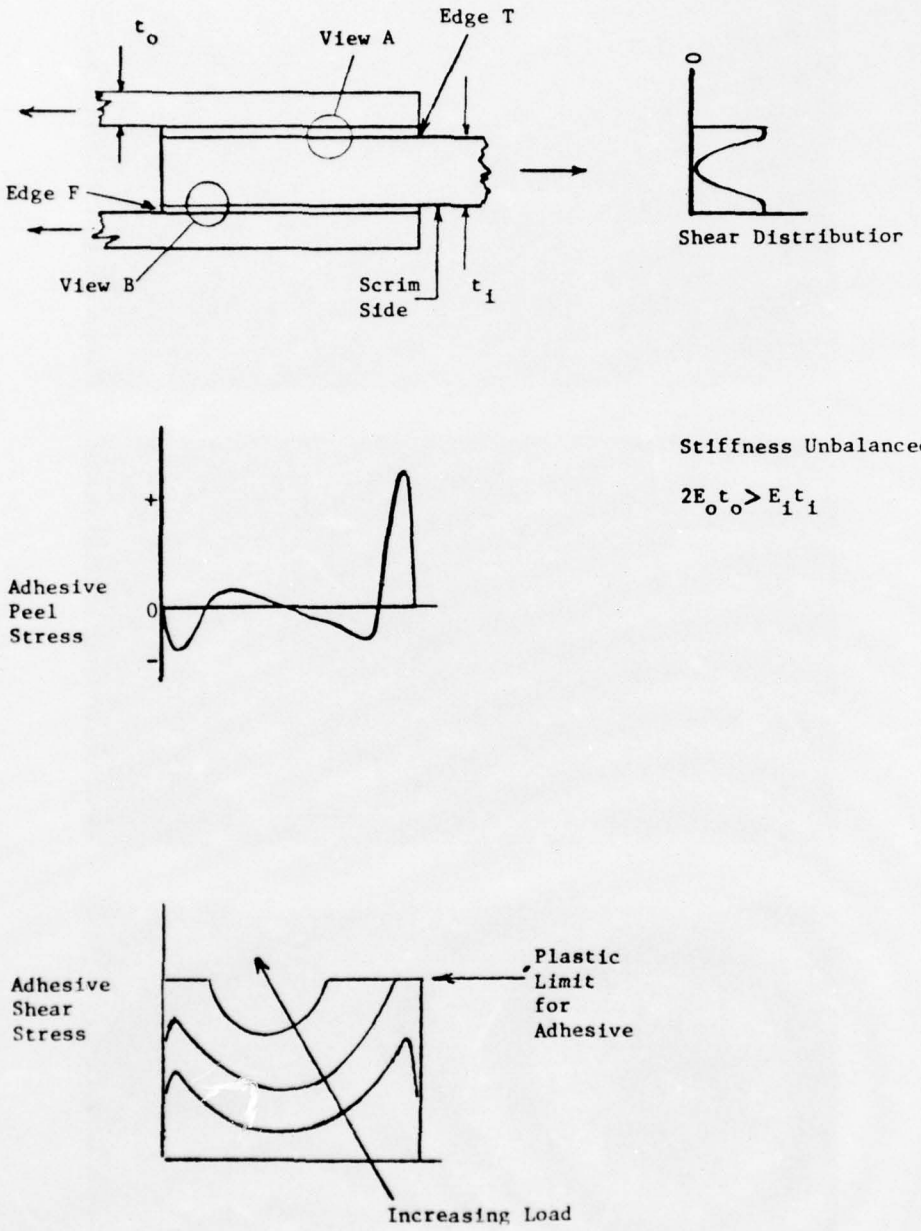

Figure I9. Stress Distributions and Ply/Scrim Stacking

AD-A042 435 AIR FORCE FLIGHT DYNAMICS LAB WRIGHT-PATTERSON AFB OHIO F/G 13/5
LOAD SPECTRUM EFFECTS ON BONDED COMPOSITE JOINTS.(U)
APR 77 R T ACHARD, M D RICHARDSON

UNCLASSIFIED AFFDL-TR-77-29 NL

2 OF 2
AD
A042435

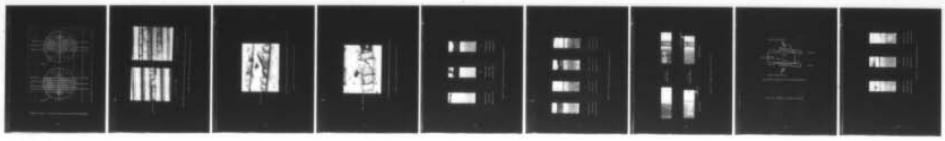

END
DATE
FILMED
8-77

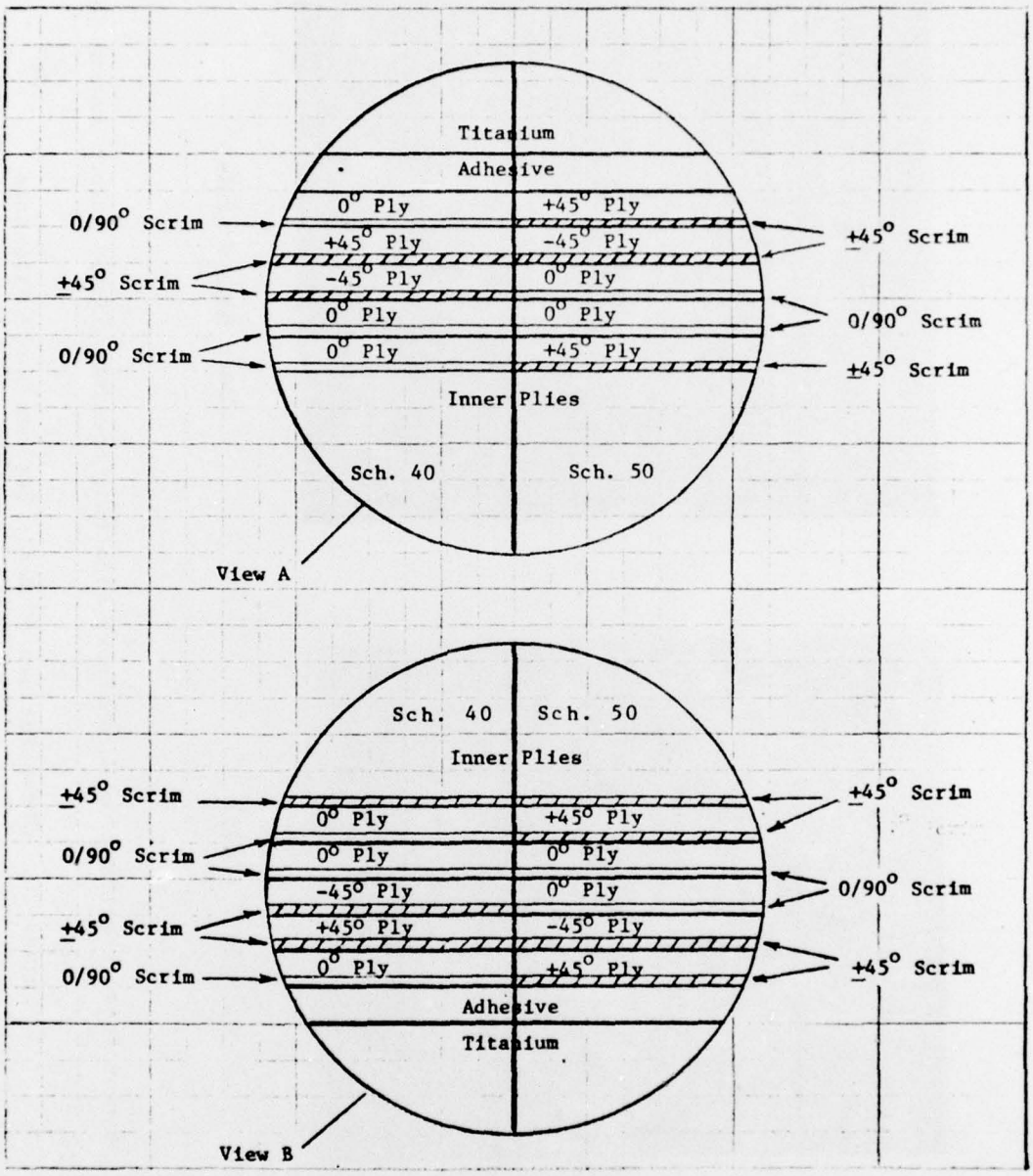

Figure 19 (cont.). Stress Distributions and Ply/Scrim Stacking

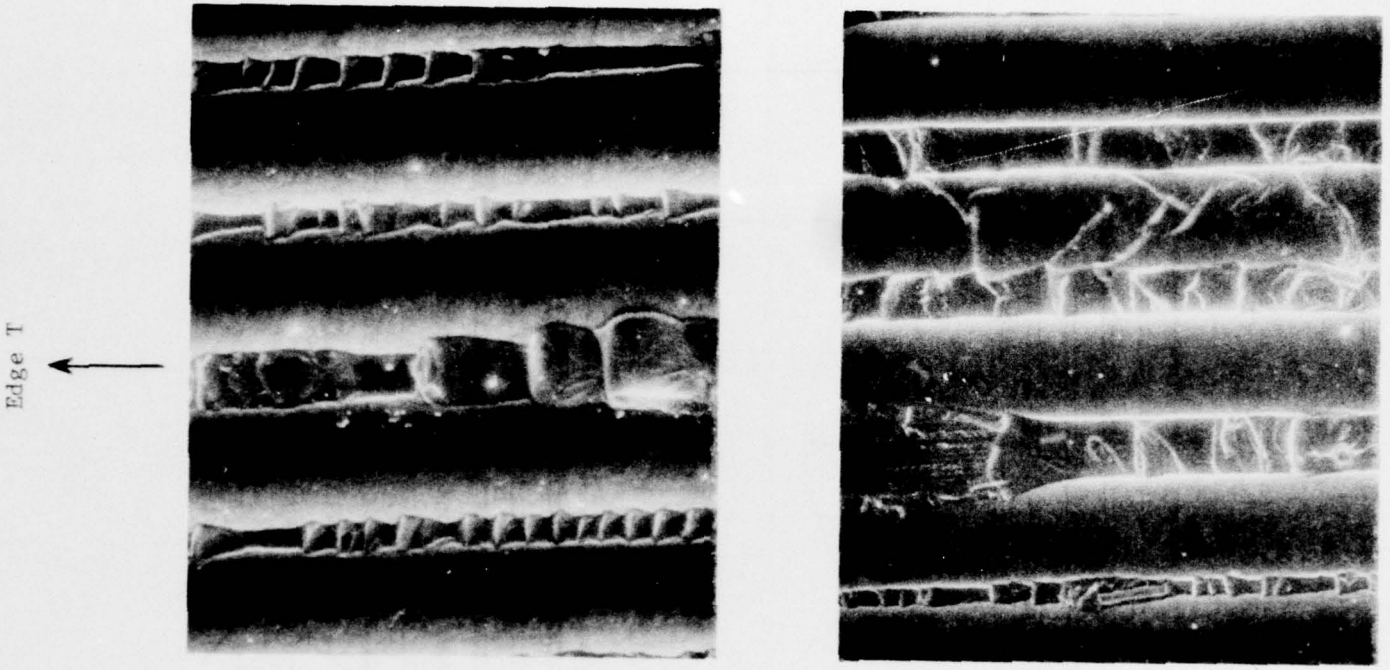

Near Edge T (200X)

Near Edge F (200X)

Note: Mode B failure surface on boron/epoxy adherend, Specimen 53-49, Select-Random test

Figure 20. Shear Failure of Resin Between Boron Filaments

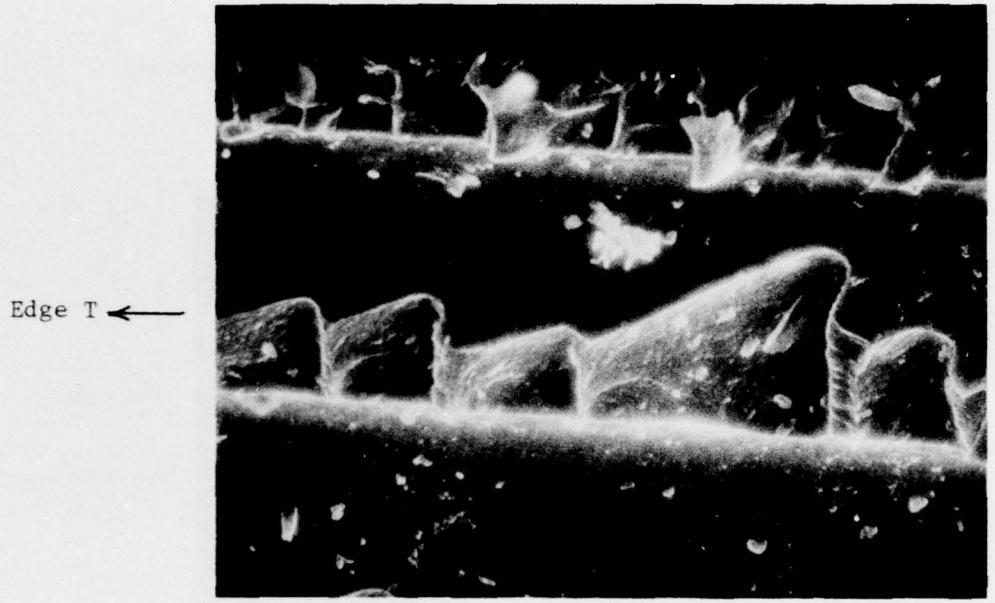

Mode B area in center of lap, Specimen 51-9, Static Test, Strap View

Figure 21. Saw Toothed Resin Fracture-Angle View.

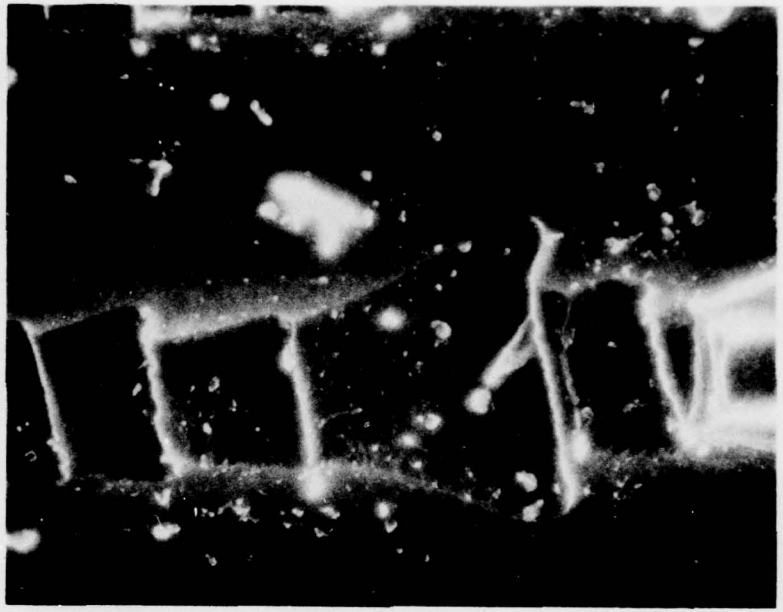

Picture taken perpendicular to fracture residue on titanium strap.

Figure 22. Saw Toothed Resin Fracture-Normal View.

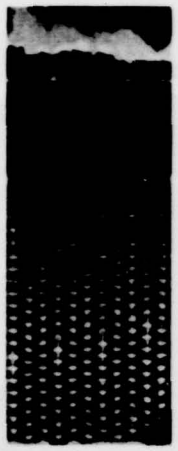

A

Pattern 40-1T

Scrim Side

Specimen 43-22

B

Pattern 40-2

Scrim Side

Specimen 42-48

C

Pattern 40-3

Scrim Side

Specimen 44-2

Figure 23. Failure Patterns for Static Tests-Schedule 40

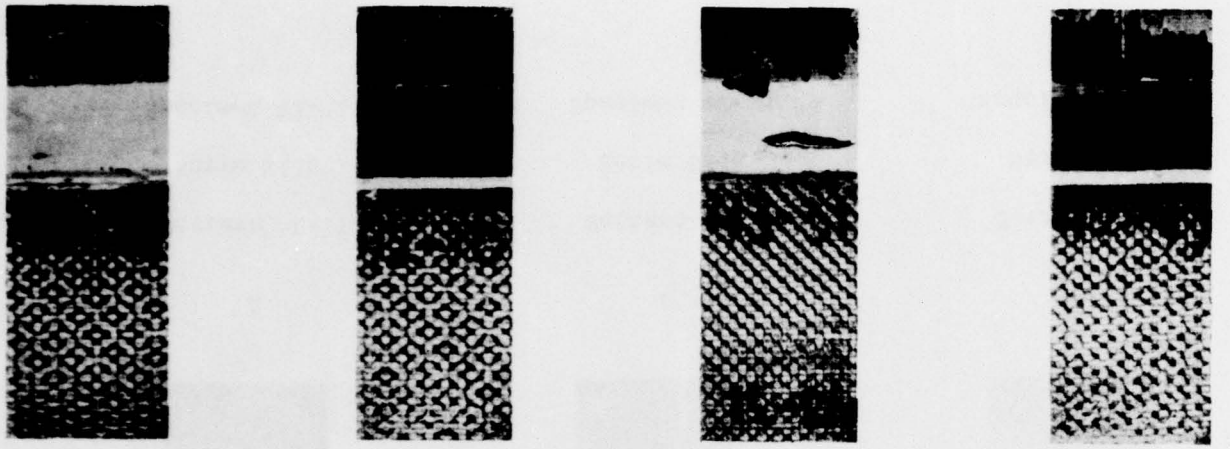

A	B	C	D
Pattern 40-2	Pattern 40-1T	Interply Failure	Pattern 40-1T
Scrim Side	Scrim Side	Nonscrim Side	Nonscrim Side
Specimen 42-28	Specimen 42-10	Specimen 43-31	Specimen 42-47

Figure 24. Failure Patterns for Fatigue-Schedule 40.

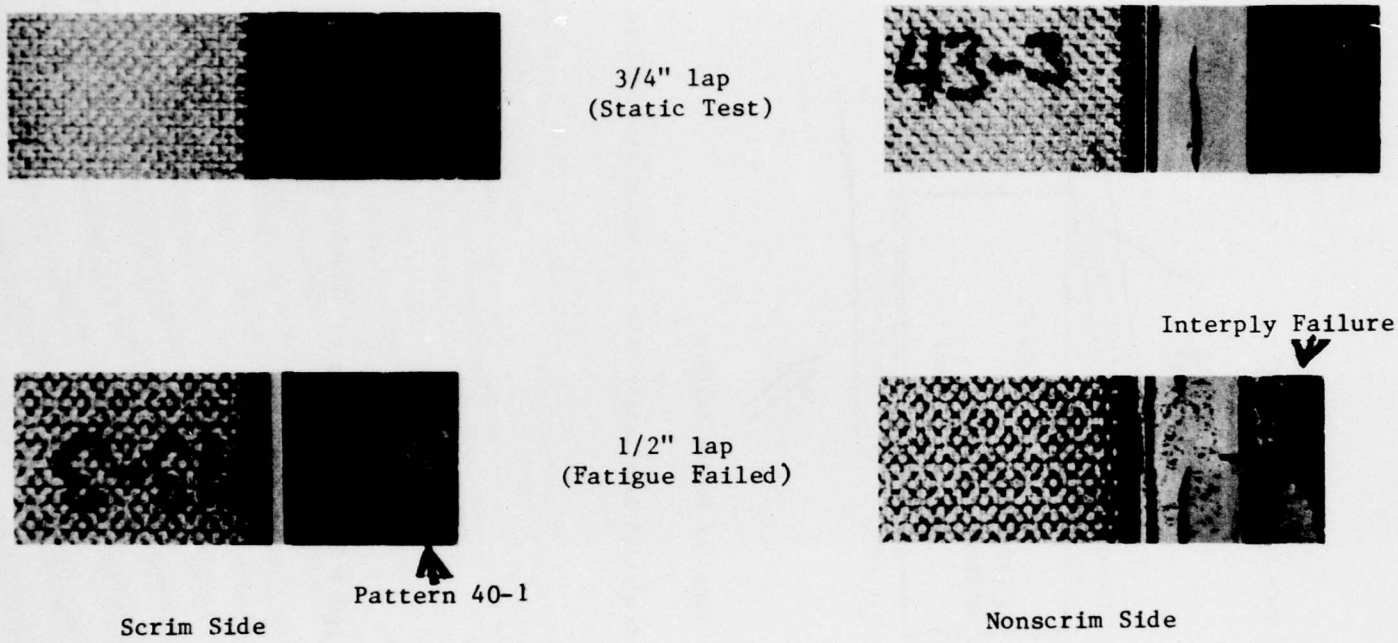

Figure 25. Fatigue Failure, 3/4 Inch Joint.

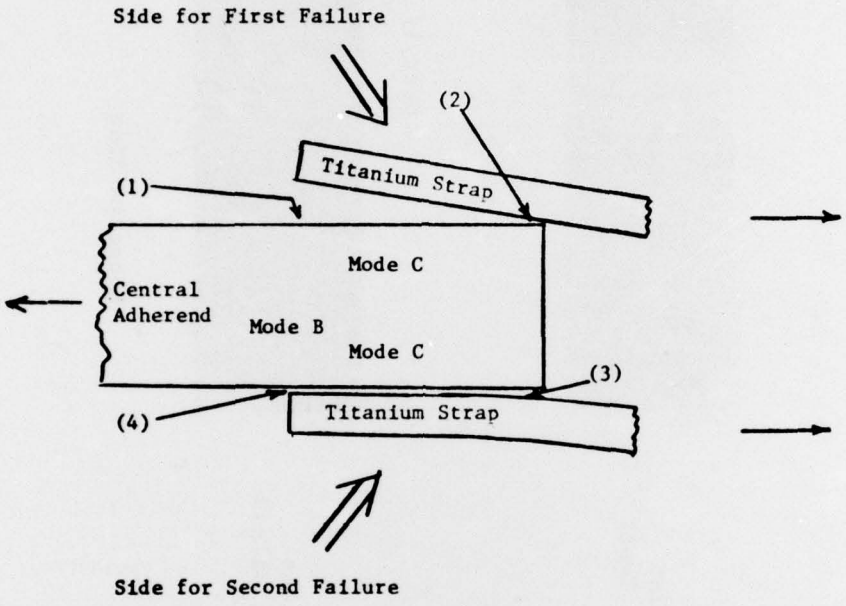

Joint Condition Immediately Prior to Second Side Failure

Figure 26. Scenario of Double Lap Failure

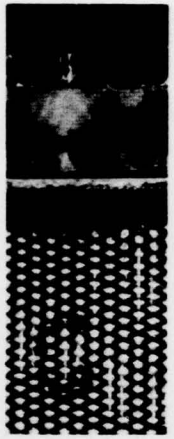

A

Pattern 50-2

Nonscrim Side

Specimen 53-22

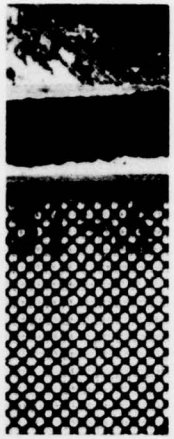

B

Mixed Mode

Scrim Side

Specimen 51-5

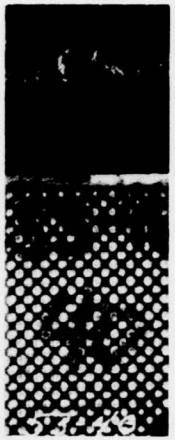

C

Pattern 50-1

Nonscrim Side

Specimen 53-46

Figure 27. Failure Patterns-Schedule 50.

☆ U. S. GOVERNMENT PRINTING OFFICE: 1977 — 757-001/480